2023

PLANT CELL WALL COMPOSITION AND *IN VITRO* FERMENTATION CHARACTERISTICS OF COOL-SEASON FORAGE GRASSES FROM TWO GROWING SEASONS IN CENTRAL KENTUCKY

Sophia Danielle Newhuis
University of Kentucky, sdnewhuis@gmail.com
Digital Object Identifier: https://doi.org/10.13023/etd.2023.137

STUDENT AGREEMENT:

I represent that my thesis or dissertation and abstract are my original work. Proper attribution has been given to all outside sources. I understand that I am solely responsible for obtaining any needed copyright permissions. I have obtained needed written permission statement(s) from the owner(s) of each third-party copyrighted matter to be included in my work, allowing electronic distribution (if such use is not permitted by the fair use doctrine) which will be submitted to UKnowledge as Additional File.

I hereby grant to The University of Kentucky and its agents the irrevocable, non-exclusive, and royalty-free license to archive and make accessible my work in whole or in part in all forms of media, now or hereafter known. I agree that the document mentioned above may be made available immediately for worldwide access unless an embargo applies.

I retain all other ownership rights to the copyright of my work. I also retain the right to use in future works (such as articles or books) all or part of my work. I understand that I am free to register the copyright to my work.

REVIEW, APPROVAL AND ACCEPTANCE

The document mentioned above has been reviewed and accepted by the student's advisor, on behalf of the advisory committee, and by the Director of Graduate Studies (DGS), on behalf of the program; we verify that this is the final, approved version of the student's thesis including all changes required by the advisory committee. The undersigned agree to abide by the statements above.

Sophia Danielle Newhuis, Student

Dr. Rachel R. Schendel, Major Professor

Dr. David Harmon, Director of Graduate Studies

PLANT CELL WALL COMPOSITION AND *IN VITRO* FERMENTATION CHARACTERISTICS OF COOL-SEASON FORAGE GRASSES FROM TWO GROWING SEASONS IN CENTRAL KENTUCKY

THESIS

A thesis submitted in partial fulfillment of the
requirements for the degree of Master of Science in the
College of Agriculture, Food and Environment
at the University of Kentucky

By
Sophia Danielle Newhuis
Lexington, Kentucky
Co-Chairs: Dr. Rachel Schendel, Assistant Professor of Food Science
and Dr. Youling Xiong, Professor of Food Science
Lexington, Kentucky
2023

ABSTRACT OF THESIS

PLANT CELL WALL COMPOSITION AND *IN VITRO* FERMENTATION CHARACTERISTICS OF COOL-SEASON FORAGE GRASSES FROM TWO GROWING SEASONS IN CENTRAL KENTUCKY

Grass cell walls are rich in cellulose, hemicellulosic arabinoxylan (AX) polysaccharides, and lignin. AX structural differences such as degree and pattern of branching and the ester-linked phenolic acid content could affect plants' digestibility when used as forage for livestock. However, there is little information about how these structural elements change over the growing season in the vegetative tissue of cool-season perennial grasses. Enhanced information about the cell wall composition and carbohydrate structure of forage material will provide a foundation for expanding our knowledge of how forage cell wall carbohydrate structures are utilized by ruminants. The objectives of this study were to investigate changes in the cell wall composition of five cool-season grasses grown in central Kentucky (perennial ryegrass (*Lolium perenne* L.), orchardgrass (*Dactylis glomerata* L.), tall fescue (*Schedonorus arundinaceus* (Schreb.) Dumort), Kentucky bluegrass (*Poa pratensis* L.), and timothy (*Phleum pratense* L.)) over the growing season and between growing years and also to explore structural carbohydrate changes in cool season forage material following fermentation with pure cultures of fibrolytic bacteria. Forages were planted in September 2019 in a randomized block design, and vegetative material was harvested in April, June, August, and October of 2020 & 2021. The collected samples were lyophilized; milled (< 0.5mm); defatted; and destarched to isolate insoluble cell wall material. The AX enzymatic fingerprint was determined by digesting cell wall material with endoxylanases and then separating and quantifying the released oligosaccharides with high-performance anion-exchange chromatography with pulsed amperometric detection (HPAEC-PAD). Phenolic acids were released via alkaline hydrolysis; extracted with diethyl ether following acidification; and separated, detected, and quantified using high-performance liquid chromatography coupled with a diode array detector (HPLC-DAD). The monosaccharide profile of the cell wall polysaccharides was determined via Saeman hydrolysis followed by HPAEC-PAD separation and detection. Lignin content was determined using the Acetyl Bromide Soluble Lignin (ABSL) method. Forage material was also incubated with pure bacterial cultures (*Fibrobacter succinogenes* (S85) and *Acetivibrio thermocellus* (27405)), and carbohydrate structural changes during fermentation were analyzed. Statistical significance was analyzed via one-way ANOVA, and Tukey-Kramer post-hoc testing was used to reveal significant pairwise differences. Incubation with selected pure cultures of fibrolytic bacteria revealed a tendency for the microorganisms to selectively remove arabinose units from the AX polysaccharides and a preference for utilization of cellulose. Reproducible seasonal changes were observed in the forage material, such as a general increase in lignin content over the growing season in both years, and an increase in ester-linked coumaric acid from the spring to summer sampling points. However other seasonal compositional changes were observed only in one sampling year, such as a significant increase in the arabinose/xylose (A/X) ratio for

most species in 2020, but not 2021, which likely reflects the different weather conditions in the two growing seasons. Other compositional elements, such as ester-linked ferulic acid, showed clear differences between species at selected sampling points, but these differences were not reproduced in the second sampling year. Taken together, these data illustrate the importance of screening multiple forage species at multiple sampling points to observe the full range of cell wall structural composition possibilities for cool-season forages and to avoid incorrect generalizations.

KEYWORDS: arabinoxylan, monosaccharide composition, HPAEC-PAD, oligosaccharide, ABSL lignin, ester-linked phenolic acids, pure culture fermentation, fibrolytic bacteria

Sophia Danielle Newhuis

(Name of Student)

April 11th 2023

Date

PLANT CELL WALL COMPOSITION AND *IN VITRO* FERMENTATION CHARACTERISTICS OF COOL-SEASON FORAGE GRASSES FROM TWO GROWING SEASONS IN CENTRAL KENTUCKY

By
Sophia Danielle Newhuis

Dr. Rachel Schendel
Co-Director of Thesis

Dr. Youling Xiong
Co-Director of Thesis

Dr. David Harmon
Director of Graduate Studies

April 11th, 2023
Date

DEDICATION

I would like to dedicate this thesis to my parents, sister, and nani. Thank you for being my biggest supporters, and for always believing in me. I would not be where I am at without each and every one of you.

ACKNOWLEDGMENTS

The following thesis, while an individual work, benefited from the insights and direction of several people. First, words cannot express my gratitude to my advisor, Dr. Rachel Schendel, for being a wonderful mentor and guide throughout this thesis. Thank you for always believing in me. Next, I wish to thank my thesis committee, Dr. Youling Xiong and Dr. Michael Flythe, who generously provided knowledge and expertise. Additionally, this endeavor would not have been possible without the generous support of the USDA-ARS, who financed my research. I am also grateful to my lab team that was always willing to help and provide support whenever it was needed. Lastly, I would like to thank my family and friends. Mom, dad, Taylor, and nani, thank you for your continuous encouragement and support.

Table of Contents

List of abbreviations

2X: Xylobiose

3X: Xylotriose

4X: Xylotetraose

5X: Xylopentose

6X: Xylohexose

A3X: α-L-arabinofuranosyl-(1→3)-β-D-xylopyranosyl-(1→4)-D-xylose

ABSL: Acetyl bromide soluble lignin

ANOVA: Analysis of variance

Ara: Arabinose

A. thermocellum: Acetivibrio thermocellum

A/X ratio: Arabinose/xylose ratio

AX: Arabinoxylan

AXOS: Arabinoxylan oligosaccharide

CO_2: Carbon dioxide

F. succinogenes: Fibrobacter succinogenes

Gal: Galactose

GH: Glycoside hydrolase

Glu: Glucose

H_2O: Water

HCl: Hydrochloric acid

HPAEC-PAD: High-performance anion-exchange chromatography paired with pulsed amperometric detection

HPLC: High-performance liquid chromatography

IVDMD: *In-vitro* dry matter digestibility

IVNDFD: *In-vitro* neutral detergent fiber digestibility

KY: KY bluegrass

MeOH: Methanol

Na_2CO_3: Sodium carbonate

NaOAc: Sodium acetate

NaOH: Sodium hydroxide

NDF: Neutral detergent fiber

OG: Orchardgrass

PAD: Pulsed amperometric detector

PAA: Peracetic acid

PR: Perennial ryegrass

PTFE: Polytetrafluoroethylene

SCFA: Short chain fatty acid

SD: Standard deviation

TF: Tall fescue

TFA: Trifluoracetic acid

Tim: Timothy

VFA: Volatile fatty acid

WSC: Water-soluble carbohydrate

XOS: Xylooligosaccharide

Xyl: Xylose

LIST OF TABLES

LIST OF FIGURES

CHAPTER 1. INTRODUCTION

1.1. Introduction to thesis

The plant cell walls of cool-season pasture grasses are rich in cellulose, hemicellulosic arabinoxylan (AX) polysaccharides, and lignin. These polymers are tightly intermeshed and, in some cases, covalently bonded, which hinders their biodegradation. The carbohydrates in grass cell walls can be degraded by a variety of native rumen microorganisms that produce various synergistic enzymes which attack specific structural elements of the cell wall polysaccharides. AX, which account for ~20% of grass biomass, contain high amounts of ester-linked phenolic acids such as ferulic acid, which, through oxidative coupling reactions, is able to cross-link AX both to itself and lignin (Grabber et al., 2009). Lignin, a complex phenolic polymer, is associated with reduced cell-wall carbohydrate degradation in mature forages, which, in grasses, has been primarily attributed to the covalent crosslinking of lignin with AX, which hinders the access of the carbohydrate-degrading enzymes to their substrates(Jung & Deetz, 1993). Ester-linked coumaric acids are also abundant in the vegetative tissue of grass species and are primarily attached to the lignin polymer, where they serve as an "oxidative shuttle" that facilitates the rapid incorporation of monolignols into an expanding lignin polymer (Hatfield et al., 2008; Lu & Ralph, 1999).

There are many structural components in the cell wall that can affect enzymatic degradability and therefore, fermentation by rumen microorganisms. The degree of branching on the AX backbone interferes with its ability to interact with cellulose via hydrogen bonding and hydrophobic interactions, as well as affecting the crystallinity of cellulose (Selig et al., 2015). With the addition of more AX branches there is less

crystallinity, making it easier to digest. The degree of crosslinking makes more physical connection points in the whole cell wall polymer network, leaving less space for microbes and their enzymes to diffuse through the material. Also, the addition of more AX-AX and AX-lignin cross-linkages will limit both chemical and physical access to the backbone (Casler & Jung, 2006). The degree and pattern of backbone substitution on the AX can vary and include additional backbone substitutions. A more densely substituted backbone containing more complex sidechains will limit enzyme accessibility (Li et al., 2013). In addition to this, each new type of glycosidic linkage that is added to the polysaccharide will require a new enzyme type that has to be produced by microbes to fully break the polysaccharide down into fermentable monosaccharide constituents (Badhan et al., 2022). Therefore, changes in cell wall structural composition can thus affect forages' digestibility for ruminant livestock and their associated microorganisms. The cell wall polymers of plants respond to abiotic stress, such as limited water, UV light, and temperature extremes with structural changes that help the plant survive (Lorenzo et al., 2018; Rakszegi et al., 2014). Additionally, the chemical structures of the cell wall polymers of many species have been shown to change as a result of plant maturity (Morrison, 1974, 1980). However, there is limited information about how the contents of the structural elements of cool-season grasses' cell walls change over the growing season.

Scattered information providing monosaccharide composition, ester-linked phenolic acid contents, and lignin content of some perennial forages has been published (Duan et al., 2021; Hatfield et al., 2009; Lam et al., 2003; Sousa et al., 2021; Xu et al., 2007). However, this data has been mostly collected in Northern Europe, and almost no

structural data exists for these forages in the transition zone of the United States, where a substantial number of beef cattle are raised. Additionally, very little data exists examining year-to-year changes in these forages' plant cell wall polymers (Lindgren & Aman, 1983; Lindgren et al., 1980; Morrison, 1974; Wallsten & Hatfield, 2016). Moreover, there are no data available that specifically look at changes in the AX structures of the vegetative material of these species over the growing seasons. Finally, pure culture studies investigating the ability of isolated fibrolytic rumen bacteria to degrade AX from perennial cool-season forages have not been reported.

The following literature review will cover 1) general AX structure in grasses, 2) the impact of AX structural variation on microbial digestion, 3) changes in the cell wall composition of cool-season forages over time, and 4) carbohydrate digestion in ruminants.

1.2 Research objectives

Grass cell walls are rich in cellulose and AX polysaccharides. Ester-linked phenolic acids such as ferulic and coumaric acids have the potential to cross-link the AX polymer both to itself and lignin. Changes in cell wall composition influence enzymatic degradability, and consequently, the microbial population of animals regularly ingesting AX-containing feedstuffs. However, limited information is available about how the contents of these structural elements of cool-season grasses' cell walls change over the growing season. Monosaccharide composition, ester-linked phenolic acid, and lignin quantification analyses of perennial forage materials collected throughout the growing season of two consecutive years provide information about changes in the ratios of cellulose, AX, and lignin in the cell walls over time as well as the degree of AX branching. Digestion of the AX in cool-season forage materials with endoxylanases

generates unique fingerprints of arabinoxylan oligosaccharides (AXOS), and the application of a validated AXOS quantification method based on this approach reveals structural changes in pasture grass AX. These same analysis methods can also be applied to forage material remaining after incubation with pure cultures of fibrolytic rumen bacteria to understand ability of these microorganisms to degrade native cell wall material of cool-season forages. This profiling of the plant cell walls of cool-season forages grown in central Kentucky will provide better structural understanding about how pasture grasses change over time and inform forage utilization practices.

The objectives of this thesis research were to 1) Investigate changes in the cell wall of five cool-season pasture grass species harvested over a four-month period across two growing seasons and to 2) Explore bacterial carbohydrate utilization in selected forage samples. To accomplish these objectives, three studies were done: 1) Cell wall compositional screening of five cool season forage species harvested over the growing season of two separate growing years, 2) Application of an enzymatic fingerprinting method to profile the AX structures of these forage materials, and 3) Pure culture fermentation of cool season forage cell wall material and exploration of cell wall composition changes.

CHAPTER 2. LITERATURE REVIEW

2.1 Grass cell wall of monocots

Plants have cell walls that are extracellular matrixes that enclose each cell in a plant. The cell walls provide a structural framework to support plant growth and provide protection to the plant. The cell wall of grasses consists of a non-lignified primary cell wall that surrounds immature cells, allowing these cells to expand and provide flexibility and structural support. The primary cell wall contains cellulose, tethering glycans or hemicellulose, which are polysaccharides that can hydrogen bond to cellulose, and pectins (Albersheim et al., 2010a). Pectins, however, are found in low abundance in grasses compared to dicotyledonous plants (see **Table 1.**). When the cell is done expanding it forms a secondary cell wall that is thicker and provides strength, allowing the plant to stand upright. The secondary cell wall includes cellulose, hemicellulose, and lignin. Lignin is a large phenolic polymer that creates a water-insoluble mesh that blankets the cell wall, blocking access to carbohydrate-digesting enzymes and reducing digestibility (Liu et al., 2018). Cellulose is an unbranched, linear polysaccharide made up of continuous β-1,4-linked glucopyranosyl residues (McDougall et al., 1996). Primary cell walls typically contain between 20-30% cellulose, while the secondary cell wall can contain up to 50% cellulose (Albersheim et al., 2010b). Hydrogen bonds formed between the β-1,4-linked chains have a strong influence on the chemical and physical nature of cellulose (Albersheim et al., 2010a). The hydrogen bonds result in lateral aggregation and crystallization of the β-1,4-linked glucan backbones into structures called microfibrils (Albersheim et al., 2010a). Hemicellulose act as tethers that link cellulose microfibrils together to form a polysaccharide network (Scheller & Ulvskov, 2010). This is done through hydrogen bonding between the unbranched regions of the hemicellulose

backbone and cellulose. As seen in **Table 1**, the cell wall composition of monocots and dicots differs. AX are the major hemicellulosic component in the cell wall of monocots, including grasses. Around 30-40% of the primary cell wall in monocotyledons is made up of AX, whereas for dicots the primary cell wall is made up of less than 5% of AX (Albersheim et al., 2010a).

Table 1. Composition of cell walls from grasses and dicots (% dry weight)[a,b]

	Primary walls		Secondary walls	
	Grasses	**Dicots**	**Grasses**	**Dicots**
Cellulose	20-30	15-30	35-45	45-50
Pectins	5	20-25	*–	–
Hemicelluloses				
Glucuronoxylan	*–	–	–	20-30
(Glucurono)arabinoxylans	20-40	5	40-50	–
Mannans	2	3-5	0-5	2-8
Xyloglucans	2-5	20-25	–	–
β-(1→3, 1→4)-glucans	2-15	–	–	–
Lignin	–	–	20	7-10

[a]Values vary between tissues and species
[b]Table modified after Vogel (2008) and Scheller and Ulvskov (2010)
*–, absent or minor

2.2 Lignin

When the cell wall is done expanding it deposits a secondary cell wall that, unlike the primary walls, includes lignin. Lignin is a complex heteropolymer derived mainly from three hydroxycinnamyl alcohol monomers, or monolignols: *p*-coumaryl, coniferyl, and sinapyl alcohols (Boerjan et al., 2003). These monolignols produce *p*-hydroxyphenyl (H), guaiacyl (G), and syringyl (S) phenylpropanoid units when incorporated into the lignin polymer (Boerjan et al., 2003). The presence of lignin increases the recalcitrance of

plant cell walls in a concentration-dependent manner (Jung & Deetz, 1993), since it behaves as a water-insoluble, polymeric blanket that coats portions of the cell wall, blocking access to cell wall carbohydrates for enzymes and reducing digestibility. Lignin in grasses is covalently connected to the hemicellulosic AX in the cell wall via oxidative coupling to ferulates. The combination of lignin's natural water-insolubility with its propensity for crosslinking with AX means that it exerts a stronger negative effect on digestibility in grass-based forages compared to dicot-based forages (for example, alfalfa) (Jung & Deetz, 1993). No obvious relationship between lignin composition (e.g. monolignol composition and polymerization pattern into either linear, "end-wise" polymers or three-dimensional, "bulk" polymers) and digestibility has emerged in the literature. However, studying this relationship is challenging due to the diversity in structure and concentration of lignin and other cell wall components even between anatomical parts of the same plants (Grabber, 2005).

2.3 Arabinoxylan structure

2.3.1 *General arabinoxylan structure*

As previously stated, AX are the major hemicellulosic component in monocots, which includes grasses and cereals, where they play a crucial structural role in the cell wall of monocots. AX interact with cellulose microfibrils via hydrogen bonding between the cellulose and unsubstituted regions of the AX backbone and also cross-link with each other and to lignin via ester-linked hydroxycinnamates, as described in the next section. Therefore, AX help to hold the cell wall structure together.

Figure 1. depicts a model AX structure, illustrating how AX's backbones consist of xylopyranose linked via β-1,4- glycosidic linkages, with arabinofuranose substituents linked to the backbone via α-1,3 and α-1,2 linkages, with both mono- and

disubstitutions observed (Scheller & Ulvskov, 2010). The majority of arabinose substituents are monomeric, but some occur as dimeric side chains consisting of two or more arabinose units coupled via α-1,2 bonds (Mazumder & York, 2010; Verbruggen et al., 1998). The degree and pattern of backbone substitution with arabinofuranose can vary, and additional backbone substitution with acetyl groups and glucuronic acid is also possible (Kabel et al., 2003; Verbruggen et al., 1998).

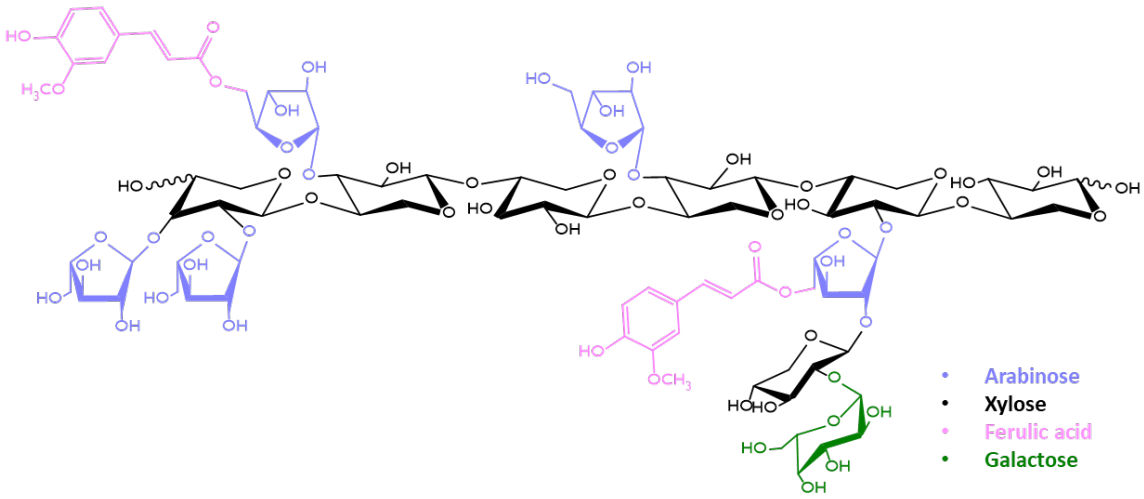

Figure 1. Structure model of feruloylated arabinoxylans from monocotyledonous plants such as grasses

2.3.2 *Hydroxycinnamic acids are esterified to arabinoxylans*

A defining feature of AX is their acylation with hydroxycinnamic acids at the *O*-5 position of arabinose substituents. The most abundant hydroxycinnamic acids found in plant cell walls from forages are *trans*-ferulic and *trans*-*p*-coumaric acids. Ferulic acid is produced via the phenylpropanoid biosynthetic pathway and is covalently linked to AX by ester bonds (Buanafina, 2009). Dimerization of ferulates is possible by photochemical coupling reactions or radical coupling (Bunzel et al., 2001). Free radical-induced oxidative coupling of ferulic acid with other ferulates, other hydroxycinnamic acids, and lignin results in covalent cross-linking of the plant cell wall polymers, forming AX-AX

and AX-lignin crosslinks (Grabber et al., 1995). Oxidative coupling between two ester-linked ferulates results in an ester/ester-linked dehydrodiferulate dimer between two AX polymers that can be released from the cell wall matrix under alkaline conditions, whereas coupling between an ester-linked ferulate and lignin results in an ester/ether-cross-coupling that requires much stronger alkaline conditions to release. Both AX-AX and AX-lignin crosslinking decrease cell wall degradability. Through these covalent linkages between polymers, the cell wall becomes more tightly networked, which affects the physical accessibility of carbohydrates to enzymes. Diferulates significantly lower the rate and extent of polysaccharide degradation because the physical access of endoxylanases to the xylan backbone is reduced, thus limiting the extent of AX degradation (Grabber et al., 1998). Enzymatic degradability is relevant for forage's utilization as nutrient carbohydrate sources in livestock systems and in feedstock for bioenergy production systems (Hatfield et al., 2017).

In contrast to ferulic acid, *para*-coumaric acid mainly acylates lignin in grasses and does not participate in oxidative coupling as readily as ferulic acid (Hatfield et al., 2017; Withers et al., 2012), meaning the coumarates do not serve as major cell wall crosslinking sites. The main role of these ester-linked coumarates is instead proposed to be acting as "oxidative shuttles" that facilitate the rapid incorporation of monolignols into an expanding lignin polymer (Hatfield et al., 2008; Lu & Ralph, 1999). Other hydroxycinnamic acids can be found in trace amounts such as caffeic and sinapic acids. All of the ester-linked hydroxycinnamic acids are able to be quantified in plant tissues following alkaline hydrolysis and solvent extraction. When plant materials or extracts are

exposed to UV light, ferulic acid and *para*-coumaric acid will isomerize from the *trans*- form to *cis*- form (Turner et al., 1991).

2.4 Arabinoxylan content and structure varies between different monocot species

2.4.1 *Arabinoxylan content varies between different monocot species*

As mentioned previously, AX are abundant in monocots such as cereal grains and forages. Research has found that AX content in monocots differs between species (Andersson et al., 2008; Gebruers et al., 2008; Shewry et al., 2010). Studies looking at the total percentage of AX in bran tissue in different varieties of wheat, barley, and rye not only found that there was variation between the different varieties, but also the species (Andersson et al., 2008; Gebruers et al., 2008; Shewry et al., 2010). Wheat bran ranged from 8.9-18.0% (Gebruers et al., 2008), barley bran ranged from 4.84-9.03% (Andersson et al., 2008), and rye bran ranged from 12.14-13.34% (Shewry et al., 2010). Not only does AX content differ in grains, but forages as well. Schadel et al. (2010) found that the total hemicellulosic concentrations in different grass leaves ranged from 10-28% of the dry grass material. (Schadel et al., 2010). Not only does the AX content differ between species, but tissues as well. When looking at the cell walls in the leaves and stems of *Brachypodium distachyon*, AX levels were lower in leaves compared to the stems (Duan et al., 2021; Rancour et al., 2012).

2.4.2 *Arabinose/xylose ratio*

The arabinose/xylose (A/X) ratio compares the molar amount of arabinose to the molar amount of xylose in AX. The A/X ratio indicates the level of substitution on the xylan backbone, and thus gives some information on how accessible the xylan backbone may be to enzymatic degradation by xylan-degrading enzymes. However, although the A/X ratio shows the total level of substitution, it provides no information about the

pattern of substitution. A/X ratios for a given species or plant tissue demonstrate a range of natural variation influenced by factors like cultivar and growing conditions (Andersson et al., 2008; Dhakarey et al., 2017; Gebruers et al., 2008; Nyström et al., 2008; Rakszegi et al., 2014), but tissue types can nevertheless be broadly differentiated by their A/X ratios (Åman, 1993; Izydorczyk & Biliaderis, 1995). In general, grain tissue of forage species tends to produce higher A/X ratios than vegetative tissue (see **Table 2.**).

Table 2. Arabinose/xylose (A/X) ratio of vegetative and grain tissues in a variety of forage species

Plant source	A/X ratio	Reference
Timothy fiber (*Phleum pretense* L.*)*	0.21-0.33	(Lindgren & Aman, 1983)
Tall fescue fiber (*Schedonorus arundinaceus* (Schreb.) Dumort)	0.17-0.26	(Lindgren et al., 1980)
Tall fescue (*Schedonorus arundinaceus* (Schreb.) Dumort) stems & sheaths	0.25	(Kasuya et al., 2008)
Orchardgrass (*Dactylis glomerata)* stem	0.24	(Kasuya et al., 2008)
Orchardgrass (*Dactylis glomerata)* stem cell walls	0.11	(Hatfield et al., 2009)
Perennial ryegrass (*Lolium perenne*) leaves	0.25-0.45	(Xu et al., 2007)
Perennial ryegrass fiber (*Lolium perenne*) leaves	0.15	(Gordon et al., 1985)
Barley (*Hordeum vulgare*) bran	0.54-0.74	(Andersson et al., 2008)
Rye (*Secale cereale*) bran	0.53-0.56	(Shewry et al., 2010)
Rye (*Secale cereale*) flour	0.66-0.76	(Nyström et al., 2008)
Durum wheat (*Triticum durum*) bran	0.70-0.80	(Gebruers et al., 2008)

2.4.3 *Amount of arabinoxylan cross-links differs between species*

Diferulates enable both AX-AX and AX-lignin cross-linking. The amount of diferulates differs between monocot species; for example, in grain tissue, corn tends to be

more heavily cross-linked compared to other grain species (Dobberstein & Bunzel, 2010). Dobberstein and Bunzel (2010) found that there was a substantially higher amount of diferulates in corn and that corn was more cross-linked, when comparing isolated fiber from commonly consumed cereal. Jilek and Bunzel (2013) examined a larger portfolio of grain species and found that popcorn had the most diferulates of all of the grains. However, in contrast to the 2010 study which had isolated the dietary fiber fraction out of the grain flours and then quantified ferulates on a dietary fiber basis, Jilek and Bunzel (2013) quantified the diferulates in the whole ground flour. Popcorn has a thick heavy shell, meaning it contains more fiber and more diferulate cross-links overall on a flour basis compared to grain corn flour. Both studies found that corn fiber is more heavily cross-linked compared to other grain species, demonstrating that AX structural differences are seen between monocot species (Dobberstein & Bunzel, 2010; Jilek & Bunzel, 2013).

2.4.4 *The number and complexity of side chains in arabinoxylans differs between species*

Not only does the content of AX differ amongst species, but the complexity does as well. As previously mentioned, the sidechains substituted to the xylan backbone on the AX structure can exhibit increased complexity with the addition of ferulate units. These feruloylated arabinose units can carry additional sugars, leading to various feruloylated di-, tri-, and tetrasaccharide branches (Allerdings et al., 2006; Appeldoorn et al., 2013; Bunzel et al., 2002). Among common cereal grains, corn AX are more complex not only because their AX structure is more heavily cross-linked, but also because their AX feruloylated side chain oligosaccharide content is higher and contains a greater percentage of the longer, more complex feruloylated oligosaccharides (Appeldoorn et al.,

2013; Jilek & Bunzel, 2013; Schendel et al., 2016). Information about how the number and complexity of side chains in AX differs between plant species is relevant for its effect on enzymatic degradation and microbial fermentation. Each additional structural component requires production of an additional accessory enzyme to fully digest the polysaccharide to its monosaccharide constituents (Rogowski et al., 2015).

2.5 Enzymatic degradability of arabinoxylan

2.5.1 *Digestion of arabinoxylan with endoxylanase releases arabinoxylan oligosaccharides*

Endo-β-1,4-D xylanases (EC 3.2.1.8, xylanases) are a specific group of enzymes within the glycoside hydrolyases (GH) family that are able to hydrolyze β-1,4 linkages of AX (Lombard et al., 2014; Pollet et al., 2010). The majority of enzymes involved in degradation of cellulose and hemicellulose come from the GH family (Krause et al., 2003). The GH family consists of sub-families which are grouped together based on their amino acid sequence and catalytic modules (Pollet et al., 2010). Most endo-β-1,4-D xylanases are categorized into the following GH families: GH 5, 8, 10, 11, 30, 43, 51, 98, and 141 (Lombard et al., 2014).

GH 10 xylanases have a broad substrate specificity and have the greatest ability to accommodate substituted AX structures among the xylanases (Pollet et al., 2010). They can cleave β-1,4 linkages on the non-reducing side of a mono- or di-substituted xylose and require only two or more unsubstituted xylose residues between branched residues for binding to and cleaving the xylan backbone (Johnny Beaugrand et al., 2004; Pell et al., 2004). Due to GH 10 xylanases being able to accommodate AX with relatively high backbone substitution rates and their high activity on xylo-oligosaccharides (XOS) with a degree of polymerization (DP) of 3 or higher, they produce mostly xylose, xylobiose, and

small substituted oligosaccharides (Pollet et al., 2010). In contrast, GH 11 xylanases, another common xylanase family, require a minimum of three unsubstituted xylose residues between branched residues for hydrolysis.

Arabinoxylan oligosaccharides (AXOS) are created once xylanase enzymes have cleaved the xylan backbone. Because endoxylanases need an unsubstituted section of xylan backbone to accomodate it in their active site, the number and distribution pattern of substituents along the xylan backbone determine the extent to which enzymes can degrade the AX (Viëtor et al., 1994). If the amount of substitution on the backbone increases, there is a corresponding decrease in the number of backbone sections that can fit into the active site of a xylanase, particularly xylanases which require three or more contiguous unsubstituted xylose residues. When wheat AX was hydrolyzed with xylanases from GH 10 and GH 11 families, different AXOS profiles were generated by the two families, reflecting the differences in the enzymes' structural requirements at their active sites (McCleary et al., 2015).

2.5.2 *Complex sidechains limit arabinoxylan digestibility*

AX from different plant sources differ in structure and complexity, which means the enzyme portfolios needed to fully hydrolyze these unique AX structures also differ. These enzymatic mixtures include xylanases and various accessory enzymes, such as β-xylosidases (EC 3.2.1.37), α-L-arabinofuranosidases (EC 3.2.1.55), α-D-glucuronidases (EC 3.2.1.139) and several esterases, including feruloyl esterase (EC 3.1.1.73) and acetylxylan esterase (EC 3.1.1.72). Enzyme mixtures that contain xylanase and other AX-degrading accessory enzymes degrade AX more efficiently than a pure xylanase (Makaravicius et al., 2012; Neumuller et al., 2014). Differences in structural complexity

also lead to different microbial fermentation patterns, since microbes need to be able to produce different enzymes to break down the polysaccharide and utilize its monosaccharide constituents for energy (Badhan et al., 2022; Feng et al., 2018; Rogowski et al., 2015).

2.5.3 *Arabinoxylan-arabinoxylan and arabinoxylan-lignin cross-links reduce carbohydrate degradability*

The main function of lignification is to provide strength and rigidity to the plant. Many studies have found that lignification of the plant cell wall matrix hinders the enzymatic breakdown of structural polysaccharides, which ultimately has a negative impact on forage utilization by livestock (Grabber, 2019; Grabber et al., 2009). However, grasses contain not only lignin, but also lignin that is cross-linked to AX (Wallsten & Hatfield, 2016).

In grasses, ferulates and diferulates are involved in the lignification process by copolymerizing with monolignols during primary and secondary cell wall formation (Grabber et al., 2009).The coupling of ferulates and diferulates with monolignols extensively interconnects the cell wall matrix by not only cross-linking AX to each other, but also cross-linking AX to lignin (Grabber et al., 2009). Previous work with corn has shown that both diferulate cross-linking of AX and AX-lignin coupling reduce cell wall degradability (Grabber et al., 1998). When fermentation of lignified versus non-lignified cell walls of corn were compared, there was a slower rate of polysaccharide fermentation and less gas production in the lignified cell walls (Grabber et al., 2009). Less gas production indicates that the polysaccharides were more difficult for the microbes to access and digest, whereas a higher amount of gas production would indicate that there is more microbial growth, therefore polysaccharides are being broken down to a greater

degree. The addition of lignin limits enzymatic access to the polysaccharides. Also, when non-lignified cell walls of corn with high vs. low amounts of AX-AX cross-links were compared, the rate of fermentation was significantly less for the material with the higher amount of crosslinking (Grabber et al., 2009). This significant decrease in fermentation rate was also seen for lignified cell walls of corn that had high amounts of AX-lignin cross-linkages compared to lignified cell walls with low amounts of AX-lignin cross-linkages (Grabber et al., 2009). This shows that higher levels of ferulates and diferulates slow carbohydrate degradability. Although this shows that lignin and ferulate cross-linking have an impact on cell wall fermentation, it is not feasible to drastically reduce the amount of lignin or AX crosslinking in forages so that the forage is easier to digest for livestock. Both lignification and AX crosslinking are vital for providing strength to the plant. However, modest reductions in lignin content of forages, as achieved through traditional breeding or transgenic approaches, have resulted in plants with improved digestibility and acceptable agronomic performance (Jung et al., 2012).

2.6 Microbial digestion of arabinoxylan is influenced by the polysaccharide structure

AX are digested by a variety of microorganisms that produce a range of hydrolytic enzymes in both ruminant and human hosts. The rate and extent of fermentation is influenced by various factors, including the microbial population's hydrolytic capabilities, the physicochemical structure of the plant material, and the AX structural complexity (Rogowski et al., 2015). Microorganisms may act either synergistically or competitively/selfishly to break down the complex polysaccharide into more metabolically accessible mono- and oligosaccharides (Feng et al., 2018).

The genus *Bacteroides* is abundant in the large intestine of humans and plays a major role in the digestion of AX (Dodd et al., 2011). *Bacteroides ovatus* is a prominent member of the human gut microbiota that is able to utilize an extensive range of plant polysaccharides. (Rogowski et al., 2015) used *Bacteroides ovatus* to investigate the xylan degrading apparatus of the genus. *Bacteroides ovatus* has a highly dynamic xylan degrading system that can readily adapt and transcribe certain GH enzymes best suited to the xylan structure based on if the xylan polysaccharide has a simple or complex substitution pattern.

2.7 Role of AX in human health and food products

Dietary fiber is the portion of plant food material that is resistant to digestion and absorption in the human small intestine with complete or partial fermentation in the large intestine (AACCI, 2001). This includes polysaccharides, oligosaccharides, lignin, and associated plant substances (AACCI, 2001). Consuming a diet rich in dietary fiber is associated with many health benefits such as reduced risk of cardiovascular disease (Jensen et al., 2004), type 2 diabetes (Chandelia et al., 2000; Hu et al., 2020; Weickert & Pfeiffer, 2018), and gastrointestinal cancer (Hullings et al., 2020; Murphy et al., 2012). As mentioned previously, AX are the major hemicellulosic component in cereal grains, therefore, they are major contributors to the dietary fiber complex in diets containing cereal grains.

2.7.1 *Prebiotic properties*

Prebiotics are defined as “a substrate that is selectively utilized by host microorganisms conferring a health benefit” (Gibson et al., 2017). AX’s prebiotic effect has been reported in both *in vitro* and *in vivo* studies (Cloetens et al., 2010; Neyrinck et al., 2011; Paesani et al., 2020). Lynch et al. (2021) used extracted brewers spent grain

that contained 99% soluble AX and found that the extracted AX showed prebiotic effects and increased *Lactobacillus* and *Bifidobacterium* levels.

2.7.2 *Functional food ingredients*

A functional food is a food that improves health and wellbeing. The various health benefits that AX offer make them an attractive additive to foods and beverages (Zannini et al., 2022). However, AX can substantially affect (both positively and negatively) the quality attributes of products in a structure-dependent fashion, so product developers must tread carefully when adding AX to products. This topic has been covered in various reviews such as (Deleu et al., 2020; Hemdane et al., 2016; Pareyt & Delcour, 2008).

2.8 Carbohydrate digestion in ruminants

A major component of ruminants' diets come from forage, either through grazing or a more conserved form such as hay or silage. Cattle are ruminant livestock, this means they have a digestive system adapted to predominantly complex carbohydrates sourced from a variety of forages (Krause et al., 2003). Their digestive system includes a distinct four-chambered stomach, consisting of the rumen, reticulum, omasum, and abomasum. The rumen is the largest part of the stomach compartment and acts as a fermentation vat and home to an expansive community of microbes that can hydrolyze and ferment fiber from forages that are indigestible to non-ruminant animals. The major fibrolytic bacteria that catalyze the degradation of fiber in the rumen are gram negative *Fibrobacter succinogenes*, and gram positive *Ruminococcus albus* and *Ruminococcus flavefaciens* (Krause et al., 2003). Volatile fatty acids are produced as a product of microbial fermentation in the rumen and are utilized by cattle as one of their main energy sources (Krause et al., 2003).

The digestibility of cell walls in forage grasses by ruminants is a limiting factor in utilization of cell wall polysaccharides as carbon and energy sources. Some cell walls can be completely digested in the rumen whereas lignified cells resist digestion (Jung et al., 2012). This reduced digestibility stems at least partially from the restricted accessibility to cellulose due to lignin encrustation for the polysaccharide-degrading enzymes produced by the rumen microorganisms (Casler & Jung, 2006). AX-lignin and AX-AX crosslinking are also associated with decreased digestibility (Casler & Jung, 2006). Additionally, AX branching patterns structures can also indirectly promote the growth of different bacterial species by hindering the bacteria's access to their preferred cell wall polysaccharides. For example, *F. succinogenes* appears to produce xylan-degrading enzymes solely for the purpose of removing AX to gain access to cellulose (Suen et al., 2011). Because AX structural differences such as extent of backbone substitution strongly affect their degradability by endoxylanases and association with cellulose microfibrils (J. Beaugrand et al., 2004; Selig et al., 2015), they will also influence the ability of this organism to hydrolyze cellulose. Plant breeding efforts targeted at improving *in-vitro* dry matter digestibility (IVDMD) of forages has tended to produce varieties with increased water-soluble carbohydrate (WSC) contents (e.g. fructans and simple sugars) and/or decreased lignin contents (Casler, 2001). Research investigating the effect of polysaccharidic cell wall components on forage digestibility, e.g. the carbohydrate constituents of neutral detergent fiber (NDF), has consistently shown a negative correlation between NDF content and IVDMD (Casler, 2001; Casler & Jung, 2006). NDF represents the plant material remaining after starch hydrolysis and washing with a neutral detergent solution which removes water-soluble carbohydrates and

proteins. NDF thus represents the insoluble cell wall material and is comprised of cellulose; water-insoluble hemicellulose, which in grasses, is made up of AX; and lignin (Van Soest & Wine, 1967). The negative relationship between NDF content and IVDMD appears to result mostly from dilution of the highly digestible WSC, and a better selection marker for direct digestibility of the insoluble cell wall material, including AX, would be *in vitro* digestibility of the NDF fraction (IVNDFD) (Casler, 2001). IVNDFD does provide an improved measure to assess digestibility of the cell wall itself, but forage breeders would also potentially benefit from even more specific structural information about forage cell wall composition to select for fine structural traits potentially associated with forage digestibility. Furthermore, because forage digestibility in ruminants is driven by the ruminant's bacteria community, a better understanding of the effects that different grass AX structures have on the growth of cellulolytic ruminant bacteria species is useful, in particular, the ability of individual microbial species to degrade more complex structural components of the polymer, and will help clarify the effects of forage inclusion on ruminants' microbial populations.

2.9 Effect of weather conditions on cell wall structure and composition

Cool-season forages' ideal growing conditions are in the spring and fall when temperatures are cooler and there is more precipitation (Ehlke & Undersander, 1990). During the summer when the temperature rises and there is less precipitation, growth is reduced. Reduction in growth of the plant will influence its chemical composition. Due to the increased weather volatility stemming from global warming, forage species may not always be grown in their ideal conditions. By being able to fully characterize the effect of extreme weather conditions on the chemical composition of forages, breeders can

develop new cultivars that are better adapted to growing in hotter temperatures and less precipitation without major loss in the cell wall components.

Various studies have shown that cell wall composition of tissue from cool-season grass species changes due to variations in weather conditions. For example, when comparing oat hulls from a harvest year where they were grown under “normal” weather conditions versus a harvest year that had less precipitation and a higher temperature, it was discovered that the chemical composition was greatly influenced by weather conditions (Schmitz et al., 2020). The oat hulls harvested in the hotter and drier year had a reduction in xylose content and a higher A/X ratio, as well as a major decrease in ester-linked ferulic and coumaric acids (Schmitz et al., 2020). These A/X results were similar to another study on drought-stressed wheat grain, which had higher AX proportions with a higher A/X ratio when compared to wheat grain grown with sufficient moisture. Increased A/X ratios in response to drought were also observed in rice leaves (Dhakarey et al., 2017; Rakszegi et al., 2014; Saulnier et al., 2012).

2.10 Previous research on changes in cell wall composition of cool-season forages over time

There is abundant literature on fine structural details of the cell wall composition of commonly cultivated grain tissues, such as corn or wheat (Ana et al., 2022; Chateigner-Boutin et al., 2016; Li et al., 2009; Marcotuli et al., 2016; Obel et al., 2002; Toole et al., 2011). Researchers have also investigated changes in grain tissue, including AX structure, over the growing season. However, there is limited research focusing on the potential changes in composition and structure of perennial cool-season forage cell walls over time (Lindgren & Aman, 1983; Lindgren et al., 1980; Morrison, 1974; Wallsten & Hatfield, 2016). Cows on pasture consume forages all year throughout the

growing season, therefore it is important to investigate the effect that harvest date may have on different cell wall components (Saulnier et al., 2012; Veličković et al., 2014).

2.11 Theoretical background for cell wall characterization methods

2.11.1 *Monosaccharide release via Saeman hydrolysis*

Acidic hydrolysis of polysaccharides to release their monosaccharide components is done to determine the monosaccharide composition of plant cell wall polysaccharides. Proper hydrolysis conditions are critical. If the material is hydrolyzed for too long, the released monosaccharides will start to degrade (Selvendran et al., 1979). Two common methods used for the hydrolysis of plant cell wall carbohydrates are methanolysis (incubation with methanolic HCl followed by TFA hydrolysis) and Saeman hydrolysis (wetting with 72% H_2SO_4 at room temperature followed by dilution with water to 1 or 2M H_2SO_4 and hydrolysis for 2-3 hours at 100ºC). Soluble plant cell wall materials (including pectins) are easily hydrolyzed with methanolysis, but crystalline cellulose is not hydrolyzed under the conditions of methanolysis, therefore Saeman hydrolysis must be used with insoluble plant cell wall material (Selvendran et al., 1979).

2.11.2 *High-performance anion-exchange chromatography (HPAEC-PAD) is ideally suited for carbohydrate separation and quantification*

Several analytical techniques are available for quantitative analysis of carbohydrates, including high-performance anion-exchange chromatography coupled to a pulsed amperometric detector (HPAEC-PAD) (Corradini et al., 2012). This analytical technique offers the advantages of high resolution and sensitivity, fast analysis, direct injection of sample without derivatization, and easy of automation (Corradini et al., 2012) Because carbohydrates are weak acids with pK_a values in the range of 12-14, at high pH

values their hydroxyl groups are partially or totally transformed into oxyanions. This allows them to be separated on anion-exchange-based columns.

2.11.3 *Quantification of ester-linked hydroxcinnamic acids*

Alkaline conditions are used to release bound ester-linked hydroxycinnamic acids from cereal grains and forages. There are many different hydrolysis parameters described in the literature (Barberousse et al., 2008; Hefni et al., 2019), but using 2M NaOH for 18 h at room temperature is the most common. Hefni et al. (2019)compared both acidic and basic hydrolyses and varied parameters such as HCl and NaOH concentrations, incubation time, and addition of enzymes during hydrolysis in hopes of optimizing a hydrolysis procedure for total phenolic acids in wheat. The highest extractability of phenolic acids was achieved using basic hydrolysis (Hefni et al., 2019). Ethyl acetate or diethyl ether can be used for the extraction of released phenolic acids following acidification because both solvents quantitatively recover free phenolic acids (Vaidyanathan & Bunzel, 2012). Caffeic acid or *o*-coumaric acid may be used as internal standards for the released phenolic acid monomers (Dobberstein & Bunzel, 2010). However, caffeic acid is detected following alkaline hydrolysis for many forage species, so it cannot be universally used.

2.11.4 *Quantification of lignin concentration in grass cell walls*

In order to accurately assess the effect of lignin on inhibition of cell wall carbohydrate utilization, lignin needs to be chemically determined with acceptable precision and accuracy. Klason lignin (KL) and acid detergent lignin (ADL) are two common methods that have been used to quantify lignin concentration in forages for years. Both methods use a concentrated sulfuric acid to digest the fibrous portion of the

forage sample, and the residue is what is analyzed for lignin (Fukushima et al., 2015). Acetyl Bromide Soluble Lignin (ABSL) is a newer method that can be used to quantify the lignin content in forages. The ABSL method solubilizes lignin in twenty-five percent acetyl bromide in acetic acid solution, and then the absorbance of the solution is read at 280 nm on a spectrophotometer. Fukushima et al. (2015) compared the three methods for quantifying lignin concentration and found that ABSL yielded the highest correlations with degradability. One disadvantage of using the KL method is that the final residue can be contaminated with materials that are not broken down in the acid hydrolysis, therefore leading to overestimation of lignin concentration. In contrast, the ADL method tends to underestimate the concentration of lignin in grass cell walls (Wallsten & Hatfield, 2016). This is due to the loss of the lignin fraction that is partially solubilized in the acid detergent step (Fukushima et al., 2021).

CHAPTER 3. MATERIALS AND METHODS

3.1 Forage sampling

Timothy (*Phleum pretense* L., cultivar "Claire"), perennial ryegrass (*Lolium perenne* L., cultivar "Linn"), Kentucky bluegrass (*Poa pratensis* L., cultivar "Ginger"), orchard grass (*Dactylis glomerata* L., cultivar "Prairie"), and tall fescue (*Schedonorus arundinaceus* (Schreb.) Dumort, cultivar "Cajun II") were planted at the Spindletop Research Farm, University of Kentucky (Lexington, KY, USA) on September 10th, 2019. Four replicate plots of each cultivar were planted in rows in a randomized block design (see **Table 4.**). The forage samples were harvested between 12 PM and 4 PM in April, June, August, and October of 2020 and 2021 with some exceptions. In 2020, perennial ryegrass was unable to be harvested in August, and KY bluegrass in October due to lack of growth. In 2021, perennial ryegrass and KY bluegrass were unable to be harvested in both August and October due to lack of growth. Plots were mowed following each harvest, meaning that each harvest represented fresh growth since the previous cutting. Within each plot, the forage was clipped to a 5 cm height from randomly chosen spots. The grass samples were harvested, immediately placed on ice, then frozen and lyophilized. The lyophilized forage samples were stored at 4ºC. Lyophilized samples were milled to <0.5 mm particle size and insoluble cell wall material was isolated via removal of water-soluble carbohydrates and destarching (refer to section 3.2).

Weather data for the 2020 and 2021 growing seasons were collected by the Soil Physics Lab at UK taken from Spindletop farm where the forages in this study were grown, and by the UK AG weather center's station. Cumulative precipitation for the two-month intervals between harvests was calculated (see **Table 3.**).

Table 3. Rain accumulation for 2020 and 2021 growing seasons

	Collection periods					
	4/20-6/20	4/21-6/21	6/20-8/20	6/21-8/21	8/20-10/20	8/21-10/21
Total rain (meters)	0.50	0.25	0.29	0.22	0.22	0.26

3.2 Isolation of water-insoluble plant cell wall material from forages

Water-insoluble plant cell wall material was collected according to Joyce et al. (2023) with minor modifications. Briefly, milled grass material (4 g per plot replicate, four plot replicates per species) was placed in a screw cap bottle (250 mL), suspended in 50 mL of phosphate buffer (0.08 M, pH 6.2) and 300 µL Termamyl SC [alpha-amylase, Novozymes]. The mixture was incubated for 20 min at 92°C in a shaking water bath (with swirling every 10 min). The samples were cooled to room temperature over ice, and the pH was adjusted to 4.5 using 0.5 M HCl. Amyloglucosidase (150 µL) was added, and samples were incubated for 30 min in a stationary water bath at 60°C (with swirling every 5 min). Samples were centrifuged (10 min, 5000 rpm), the supernatant was carefully removed, and the pellet was washed twice with water (60°C, 1×100 mL and 1×50 mL), three times with ethanol (2×100 mL and 1×50 mL), and three times with acetone (2×100 mL and 1×50 mL). The supernatant was discarded between each step. The samples were placed in a fume hood for 48 h to volatilize the acetone. Then the samples were dried in a drying oven (60°C) overnight, and then placed in a vacuum oven for 48 h (90 mbar, 70°C). The samples then were stored in a dessicator until analysis.

3.3 Monosaccharide analysis of insoluble cell wall material

The monosaccharide profile of the insoluble cell wall material was determined and analyzed as described in Joyce et al. (2023) with minor modifications, using Saeman

hydrolysis conditions (Saeman et al., 1945). Briefly, dried water-insoluble grass cell wall material (100 mg) was weighed into a 50 mL glass Pyrex tube along with glass beads, 1.5 mL of 12 M H_2SO_4 was added, and the material was vortexed for 1 min. Samples were placed on ice for 30 min, vortexing for 1 min every 10 min. Samples stood out at room temperature for 2 h, vortexing for 1 min every 30 min. Each sample was diluted with water (9.75 mL), vortexed for 1 min, and placed in a drying oven (100°C) for 3 h. After cooling, the sample was filtered through a polytetrafluoroethylene (PTFE) syringe filter (0.22 μm pore size) and 5 mL of filtrate were added into a new 50 mL glass pyrex tube with 40 mL of water. The filtrate was neutralized with 4M NaOH (3.3 mL, add dropwise until pH ranges between 5-7). Samples were diluted 1:20 prior to HPAEC-PAD injection. Diluted samples were separated on a CarboPac PA-1 anion-exchange column (250 × 4 mm; Thermo Scientific Dionex) preceded by a guard column (4 × 50 mm) in an ICS-5000+ HPAEC-PAD system from Thermo Scientific Dionex equipped with an AS-AP autosampler, dual pump, and DC electrochemical detector. The injection volume was 25 μL, and the flow rate was 1 mL/min with a ternary gradient (eluent A: deionized water; eluent B: 0.1 M NaOH stored under a headspace blanket of nitrogen gas; eluent C: 0.2 M NaOAc in 0.1 M NaOH and stored under a headspace blanket of nitrogen gas; gradient conditions at injection 90 % A, 10 % B, 0 % C; linear from 0-1.5 min following sample injection to 96 % A, 4 % B, 0 % C; hold until 25 min; linear from 25-35 min to 0 % A, 100 % B, 0 % C; abrupt change to 0 % A, 0 % B, 100 % C; hold from 25-35 min; abrupt change to 0 % A, 100 % B, 0 % C; hold from 45-55 min; abrupt change to 90 % A, 10 % B, 0 % C; hold from 55-65 min). A quadruple potential detector waveform was implemented [“carbohydrate (standard quad)”] with a gold working electrode, and both

the column and detector compartments were heated to 30 °C. Five-point standard calibration curves were created from monosaccharide standard compounds for two concentration ranges (1-25 μM and 25-125 μM) for the main sugars released in the grass samples by hydrolysis (arabinose, galactose, glucose, and xylose). The resulting chromatographic data were analyzed using the Chromeleon software program (Thermo Scientific Dionex) and peak areas were fitted to quadratic curves in Origin (Pro), (version 2017; OriginLab Corporation, Northampton, MA, USA). The complete analysis was performed in quadruplicate (four biological replicates, one from each plot) for each grass species.

3.4 Determination of ester-linked phenolic acid content

Hydroxycinnamic acids were isolated from insoluble cell wall material via alkaline hydrolysis, followed by acidification and ether extraction according to Joyce et al. (2023) with minor modifications. Briefly, dried water-insoluble material (100 mg) was weighed into a 50 mL glass Pyrex tube with an open top screw cap that had silica/PTFE faced filters in the cap. 5 mL of 2 M NaOH was added and the sample was vortexed for 1 min. Internal standard (50 μL of 5 mM *trans*-*o*-coumaric acid) and a magnetic stir bar were added to each tube, and samples hydrolyzed for 18 h in the dark with constant stirring. Samples were acidified to pH < 2 with 2 mL of 12 N HCl. The ester-linked phenolic acids were extracted three times with diethyl ether (6 mL, 5 mL, 5 mL). For each extraction, samples were centrifuged to separate the organic and aqueous layers, and the organic layer was collected and combined for each replicate. Ether extracts were evaporated to dryness under N_2 stream. Dried residues were dissolved in 1 mL MeOH/H_2O (50/50 v/v). Samples were diluted 1:10 in 250 μM ortho-coumaric acid solution prepared in MeOH/H_2O (50/50 v/v) prior to HPLC analysis with diode-array

detection (DAD) using a Shimadzu 20-AR system equipped with a SIL-20AHT autosampler, two LC-20AT pumps, and an SPD-M20A photodiode array detector. Samples (10 μL injection volume) were separated on a Phenomenex Luna phenyl-hexyl column (250 × 4.6 mm, 5 μm particle size) using the following binary gradient: eluent A = 1 mM TFA; eluent B = [90/10 v/v (acetonitrile)/(1 mM TFA in 50/50 v/v MeOH/H_2O)]; gradient condition at injection 88 % A, 12 % B; hold for 13 min; linear from 13-23 min from 12 to 15 % B; hold from 23-28 min, linear from 28-33 min from 15 to 16 % B; linear from 33-37 min from 16 to 66 % B, hold from 37-42 min, linear from 42-43 min back to starting conditions of 88 % A, 12 % B; with re-equilibration for 10 min. Compounds were detected at 325 nm and quantified with linear, equidistant, 6-point internal calibration curves (*trans*-ferulic and *trans*-*p*-coumaric acid, 100-1000 μM; *cis*-ferulic and *cis*-*p*-coumaric acid, 10-100 μM and 7-70 μM, respectively), using *ortho*-coumaric acid as the internal standard (250 μM).

3.5 Lignin analysis

The lignin content of the insoluble cell wall material was determined using the acetyl bromide soluble lignin (ABSL) according to Barnes and Anderson (2017) with minor modifications. Briefly, the dried water-insoluble material (50 mg) was placed in a 2 mL centrifuge tube, 1 mL 70% ethanol was added, the sample was vortexed for 1 min, and the supernatant was removed. 1 mL of 1:1 chloroform: methanol was added to the tube, vortexed for 1 min, and the supernatant was removed. 1 mL of acetone was added, the sample was vortexed for 1 min, supernatant was removed, and the material was dried in the fume hood overnight with caps open (remaining material is AIR). To destarch the AIR, 1 mL 90% DMSO was added to pellet, vortexed for 1 min, and placed in a platform rocker (50 rpm) to shake overnight. The next day the pellet was centrifuged and the

supernatant was removed. The pellet was washed once with 1 mL 90% DMSO, vortexed for 1 min, centrifuged, and the supernatant was removed. Then the pellet was washed six times with 1 mL 70% ethanol, vortexed for 1 min, centrifuged, and the supernatant was removed. 1 mL acetone was added to the pellet, vortexed for 1 min, centrifuged, and supernatant was removed. The material air dried in the fume hood overnight and this material was the destarched AIR. The destarched AIR (5 mg) was placed in a 50 mL glass pyrex screw cap vial, 1 mL of 25% acetyl bromide added (1 mL 25% acetyl bromide added to empty tube to serve as blank), tubes were gently swirled, and placed in a water bath (50 °C) for 2 h with gentle swirling every 10 min. The samples were placed on ice to cool and 5 mL of glacial acetic acid was added to stop the reaction. Once cooled, samples were vortexed for 1 min. The residual AIR was placed in the fume hood overnight to allow it to settle to the bottom. Making sure not to re-suspend the residual AIR, 300 µL of acetyl bromide solution was transferred to a glass open top tube, and 400 µL of 1.5 N NaOH was added. Then 300 µL of 0.5 M (freshly made) hydroxyalamine hydrochloride was added. The mixture was diluted with 1 mL glacial acetic acid, and 800 µL of this solution was added to a clean quartz cuvette. The sample was read on a spectrophotometer at 280 nm, and the absorbance was recorded. Beer's Law was used to calculate the percentage of ABSL with an extinction coefficient of 17.75 g^{-1} L cm^{-1} (Barnes & Anderson, 2017) and a path length of 1 cm.

3.6 AXOS fingerprinting method

The method used for the AXOS fingerprinting was taken from (Joyce et al., 2023). A working enzyme solution (12.5 U/mL) of *Cellvibrio japonicus* (Megazymes, Bray, Ireland) was freshly prepared in water. The dried water-insoluble cell wall material (30 mg, section 3.2), 24 µL of working enzyme solution, and 1176 µL of D.I water were

added to 2 mL Eppendorf tube with a screw cap. Samples were incubated in a thermoshaker dry bath (Grant Instruments PHMT-PSC24) for 12 h (60°C, 600 rpm). Samples were placed in a hot water bath (95°C) for 15 min following incubation to deactivate enzymes. Samples were centrifuged at 1400 rpm for 10 min. An aliquot (500 µL) of supernatant was removed, mixed with 1 mL of water, filtered through PTFE syringe filter (0.22 µm pore size), lactose was added as internal standard, and analyzed via optimized HPAEC-PAD method from (Joyce et al., 2023). Released oligosaccharides were identified by comparing peak retention times with authentic standard compounds (see **Figure 6.**) and quantified using quadratic calibration curves. A new set of calibration curves was measured on the HPAEC-PAD with each new batch of eluent.

3.7 Pure culture fermentation

Perennial rye harvested in April of 2020 was used as the fermentation substrate for the pure culture incubation study. The two bacterial species used were *Fibrobacter succinogenes* (S85), and *Acetivibrio thermocellus* (27405). The cultures were grown on cellulose paper and then transferred to ball mill cellulose. *F. succinogenes* was grown in celluloytic defined media (PC + VFA + PAA) (refer to section 7.2.5.1) and *A. thermocellus* was grown on thermophile medium (T. medium) (refer to section 7.2.5.2). A bacteria-free control (media and grass material) was also incubated. The dried water-insoluble plant cell wall material (125 mg or 150 mg depending on amount of sample material) and media (6.25 mL for 125 mg, 7.5 mL for 150 mg) were added to Balch tubes (should equal out to be 2% substrate and 10% inoculum). The samples were incubated for 5 days in a water bath (63°C, 100 rpm for *A.thermocellus* or 39°C, 100 rpm for *F. succinogenes*). Following incubation, samples were centrifuged, and 3 mL of supernatant was collected. The remaining sample was transferred to 15 mL plastic conical tubes, 6-

7.5 mL of water added to Balch tubes to collect remaining sample (final volume 10 mL). The samples were centrifuged at 15,000 *g* for 10 min and remaining supernatant was collected. Then 5 mL water was added, and samples were centrifuged two times, with supernatant being removed each time. All fractions were frozen in -20°C freezer, and the pellet was freeze-dried for 7 days. A monosaccharide analysis following Saeman hydrolysis (refer to section 3.3) and AXOS fingerprinting (refer to section 3.6) were done on the pellet material to determine the monosaccharide composition and AXOS fingerprint following fermentation.

3.8 Experimental design and statistical analysis

Four replicate plots of each cool-season forage cultivar were planted in September 2019, and cultivar plots were arranged in a randomized block design (see **Table 4.**). The forage plots were mowed prior to each harvest so that the plots could experience four weeks of fresh growth. At each harvest, some species had plots that were unable to be harvested due to lack of growth. These plots were April (105 Kentucky bluegrass, 205 tall fescue), June (102 orchard grass), and August (102 orchard grass, 406 timothy) for 2020. For 2021, June (201 Kentucky bluegrass), and October (301 timothy, 406 timothy). In 2020, perennial ryegrass was not harvested in August and KY bluegrass in October due to lack of growth for all four plots. In 2021, both perennial ryegrass and KY bluegrass were unable to be harvested in August or October due to lack of growth for all four plots.

Table 4. Layout of cool-season forage plots at UK Spindletop farm

Plot # and cultivar			
101 Cajun II	201 Ginger	301 Clair	401 Linn
102 Prairie	202 Clair	302 Cajun II	402 Prairie
103 Clair	203 Prairie	303 Linn	403 Cajun II
104 Linn	204 Wrangler	304 Ginger	404 Wrangler
105 Ginger	205 Cajun II	305 Prairie	405 Ginger
106 Wrangler	206 Linn	306 Wrangler	406 Clair

Bermuda grass (this species was not studied in this thesis) cultivar "Wrangler", Kentucky bluegrass cultivar "Ginger", orchard grass cultivar "Prairie", perennial ryegrass cultivar "Linn", tall fescue cultivar "Cajun II", and timothy cultivar "Clair"

Changes in molar proportions of cell wall monosaccharides, concentrations of ester-linked phenolic acids, concentrations of lignin, and concentrations of xylose and individual oligosaccharides following endoxylanase digestion measured at four time points in 2020 and 2021 for five cool-season forages (n=4, with the exception of the species that had plots that were unable to be harvested due to insufficient growth), were evaluated using one-way analysis of variance (ANOVA) according to ANOVA: single factor in Microsoft Excel (2016). If significant differences (p <.05) were seen, means were compared using Tukey-Kramer Post Hoc test performed in SAS (version 9.4; SAS Inst. Inc, Cary, NC), Microsoft Excel (2016), or Origin (Pro), (version 2017; OriginLab Corporation, Northampton, MA, USA). Effects of species differences (n=5, with the exception of the species that were unable to be harvested at certain time points due to insufficient growth) in molar proportions of cell wall monosaccharides, concentrations of ester-linked phenolic acids, concentrations of lignin, and concentrations of xylose and individual oligosaccharides following endoxylanase digestion were determined by one-way ANOVA according to ANOVA: single factor in Microsoft Excel (2016). If significant differences (p <.05) were seen, means were compared using Tukey-Kramer

Post Hoc test performed in SAS (version 9.4; SAS Inst. Inc, Cary, NC), Microsoft Excel (2016), or Origin (Pro), (version 2017; OriginLab Corporation, Northampton, MA, USA). Effects of pure culture fermentation using perennial ryegrass harvested in April 2020 (n=3) on molar proportions of cell wall monosaccharides and concentrations of xylose and individual oligosaccharides following endoxylanase digestion were evaluated using one-way ANOVA according to ANOVA: single factor in Microsoft Excel (2016). If significant differences (p <.05) were seen, means were compared using Tukey-Kramer Post Hoc test performed in Microsoft Excel (2016). A Pearson's correlation coefficient analysis (PROC CORR) for total lignin content and total ester-linked coumarates (n=67) was done in SAS (version 9.4; SAS Inst. Inc, Cary, NC) for both the 2020 and 2021 harvest years (see section 3.4**, Table 9.**).

CHAPTER 4. RESULTS AND DISCUSSION

4.1 Monosaccharide analysis of insoluble cell wall material

See section 3.3 in methods.

The monosaccharide composition of the water-insoluble plant cell wall material was analyzed after H_2SO_4 hydrolysis according to method by Saeman et al. (1945) and quantified via HPAEC-PAD. Arabinose, galactose, glucose, and xylose were found in all five forage species (see **Table 5.**). These results are presented as molar ratios rather than absolute amounts due to the incomplete hydrolysis of insoluble cell wall material in the Saeman method. Glucose was the dominating monosaccharide in all five forages. There was a clear tendency for an increase in the proportion of arabinose for 2020 and 2021. The proportion of arabinose in perennial ryegrass increased from 9-11% and for tall fescue 6-9% over the 2020 growing season. In 2021, the proportion of arabinose in tall fescue increased from 7-9% from June to October. Several species also had an increased proportion of galactose over the growing season, particularly in 2020. Specifically, timothy (2-4%), tall fescue (1.8-2.4%), and perennial ryegrass (2-5%). The proportion of glucose corresponding to cellulose decreased in April compared to the other harvest months in tall fescue and perennial ryegrass in 2020. This indicates that the proportion of cellulose would be lower in the cell walls of those forages in April. Timothy, orchard grass, and KY bluegrass did not have any significant changes in the proportion of glucose in the 2020 growing season. There was no overarching trend seen for xylose. The xylose content increased in the June and August 2020 collection points for tall fescue, whereas for orchard grass, a steady decrease in xylose was seen. In 2021, tall fescue had an increase in the proportions for xylose in the warmer months. In contrast, the proportions of xylose in KY bluegrass tended to decrease.

Table 5. Molar percentages of monosaccharides released via Saeman hydrolysis from insoluble cell walls of cool-season forages

Harvest year	Forage species	April		June		August		October	
2020		mean	SD	mean	SD	mean	SD	mean	SD
	Timothy								
	Ara	9.7[a]	0.7	9.5[a]	0.7	11.7[a]	3.5	11.5[a]	0.6
	Gal	3.1[a,b]	1.0	2.6[a]	0.4	4.6[b]	1.0	4.0[a,b]	0.4
	Glu	54.1[a]	3.1	54.0[a]	1.1	48.2[a]	6.8	54.7[a]	1.5
	Xyl	33.1[a]	2.7	33.9[a]	0.7	35.4[a]	9.4	29.9[a]	2.4
	Tall fescue								
	Ara	7.0[a]	0.2	7.1[a]	0.5	8.7[b]	0.3	9.0[b]	0.6
	Gal	1.8[a]	0.0	1.8[a]	0.2	2.2[a,b]	0.2	2.4[b]	0.2
	Glu	52.7[a]	0.7	49.9[b]	0.9	48.8[b]	0.5	48.9[b]	0.8
	Xyl	38.6[a]	0.5	41.3[b]	0.4	40.3[b,c]	0.3	39.6[a,c]	1.2
	Orchard grass								
	Ara	7.9[a]	0.1	8.5[b]	0.3	9.0[b]	0.3	8.7[b]	0.3
	Gal	2.7[a]	0.3	2.7[a]	0.1	2.6[a]	0.4	2.9[a]	0.1
	Glu	52.4[a]	1.4	53.9[a]	1.3	55.0[a]	2.1	55.9[a]	0.9
	Xyl	37.0[a]	1.3	34.9[a,b]	1.5	33.4[b]	1.9	32.5[b]	1.3
	KY bluegrass								
	Ara	9.1[a]	0.4	9.2[a]	0.4	11.1[b]	0.4		
	Gal	2.7[a]	0.3	3.2[b]	0.3	3.8[c]	0.2		
	Glu	53.5[a]	0.5	53.5[a]	1.2	52.6[a]	0.6		
	Xyl	34.8[a]	1.0	34.2[a]	0.7	32.4[b]	0.3		
	Perennial ryegrass								
	Ara	7.0[a]	1.3	8.2[a]	0.7			12.6[b]	0.4
	Gal	2.6[a]	0.38	3.2[a]	0.42			5.3[b]	0.2
	Glu	58.4[a]	3.6	54.8[a]	1.0			50.5[b]	0.7
	Xyl	32.0[a]	2.4	33.7[a]	1.4			31.6[a]	1
2021									
	Timothy								
	Ara	11.0[a]	1.5	10.6[a]	1.0	13.1[a]	2.05	10.6[a]	0.3
	Gal	3.8[a]	1.0	3.1[a]	0.4	5.0[a]	2.07	3.2[a]	0.2
	Glu	51.6[a]	7.5	55.4[a]	1.33	50.4[a]	11.99	57.0[a]	0.2
	Xyl	33.5[a]	7.4	30.9[a]	0.35	31.4[a]	7.91	29.3[a]	0.8

Tall fescue								
Ara	8.3[a]	0.6	8.0[a]	0.4	9.4[b]	0.3	9.2[b]	0.2
Gal	2.5[a,b,c]	0.3	2.3[b]	0.1	2.8[c]	0.2	2.7[a,b,c]	0.1
Glu	50.8[a]	0.6	49.9[a]	0.9	49.6[a]	1.2	51.0[a]	0.3
Xyl	38.4[a,b]	1.0	39.8[b]	0.8	38.2[a,b]	1.5	37.0[a]	0.2
Orchard grass								
Ara	8.9[a]	0.6	8.6[a]	0.1	9.4[a]	0.3	9.0[a]	0.5
Gal	2.4[a]	0.2	2.1[b]	0.1	2.2[a,b]	0.1	2.4[a]	0.1
Glu	54.1[a]	0.6	55.2[a]	1.2	54.7[a]	0.7	54.5[a]	1.1
Xyl	34.6[a]	0.7	34.1[a]	1.2	33.8[a]	0.6	34.0[a]	1.1
KY bluegrass								
Ara	8.9[a]	0.8	8.8[a]	0.2				
Gal	2.7[a]	0.3	2.9[a]	0.1				
Glu	52.9[a]	0.4	54.2[b]	0.4				
Xyl	35.6[a]	1.1	34.1[a]	0.5				
Perennial ryegrass								
Ara	9.0[a]	0.6	9.4[a]	0.8				
Gal	3.3[a]	0.1	3.8[a]	0.6				
Glu	56.0[a]	3.8	55.7[a]	0.5				
Xyl	31.7[a]	4.3	31.1[a]	0.9				

Means with different letters in the same row are statistically different between species ($p < 0.05$); means with shared letters in the same row are statistically equivalent.
Abbreviations: Ara: arabinose, Gal: galactose, Glu: glucose, SD: standard deviation, and Xyl: xylose

4.2 Arabinose/xylose ratio of insoluble cell wall material

The A/X ratio indicates how substituted the xylan backbone is. If the ratio for the grasses is low, it would match what was previously found in literature (Gordon et al., 1985; Hatfield et al., 2009; Kasuya et al., 2008; Lindgren & Aman, 1983; Lindgren et al., 1980; Xu et al., 2007). The differences in the proportions of arabinose and xylose in the

forages an increase in the rate of backbone substitution (see **Table 6.**). The A/X ratio nearly doubled from April to October in 2020 for perennial ryegrass. There also was a significant increase ($p < .05$) over the 2020 growing season for tall fescue, orchard grass, and KY bluegrass. In contrast, for 2021 although A/X ratios increased slightly for tall fescue, there were no significant changes in backbone rate substitution. These differences between the two growing seasons on whether the backbone substitution rate was affected could be due to weather conditions. Some studies have reported that drought-stressed plants tend to produce more AX with a lower degree of substitution compared to well-watered plants (Dhakarey et al., 2017; Fanuel et al., 2022; Rakszegi et al., 2014). Higher substitution levels permit water diffusion, meaning water could escape out of the cell (Saulnier et al., 2012). In drought conditions, plants use AX to help control their tissue hydration levels and adjust the level of substitution on the AX polymer to control water from leaving the plant cell (Saulnier et al., 2012). The 2020 growing season had more rain accumulation (see **Table 3.**). Schmitz et al. 2020 saw an opposite trend however, reporting that the A/X ratio was lower in oat hull samples collected from drought-stressed plants compared to plants receiving adequate moisture.

Table 6. Arabinose to xylose (A/X) ratio of insoluble cell wall material of cool-season forages

Harvest year	Forage species									
2020	**Timothy**		**Tall fescue**		**Orchard grass**		**KY bluegrass**		**Perennial rye**	
	mean	SD	mean	SD	mean	SD	mean	SD	mean	SD
April	0.29[a]	0.04	0.18[a]	0.00	0.21[a]	0.01	0.26[a]	0.02	0.22[a]	0.03
June	0.28[a]	0.02	0.17[a]	0.01	0.24[a,b]	0.02	0.27[a]	0.01	0.24[a]	0.03
August	0.36[a]	0.17	0.22[b]	0.01	0.27[b]	0.02	0.34[b]	0.01		
October	0.39[a]	0.05	0.23[b]	0.02	0.27[b]	0.02			0.40[b]	0.02
2021										
April	0.34[a]	0.10	0.22[a]	0.02	0.26[a]	0.02	0.25[a]	0.03	0.29[a]	0.05
June	0.34[a]	0.03	0.20[a]	0.01	0.25[a]	0.01	0.26[a]	0.01	0.30[a]	0.03
August	0.43[a]	0.04	0.25[b]	0.02	0.28[a]	0.01				
October	0.36[a]	0.02	0.25[b]	0.01	0.27[a]	0.02				

Means with different letters in the same column are statistically different between species ($p < 0.05$); means with shared letters in the same column are statistically equivalent.
Abbreviations: SD: standard deviation

3.4 Hydroxycinnamic acid profile of insoluble cell wall material

See 3.4 for methods

The insoluble cell wall material of five cool-season grasses contained ester-linked *trans*-ferulic, *cis*-ferulic, *trans-p*-coumaric, *cis-p*-coumaric acids. The total levels of monomeric ester-linked phenolic acids were between 5,000-10,000 µg g^{-1} water-insoluble cell wall material for 2020 and 2021 (refer to **Tables 7. and 8.**). The *cis*- and *trans*-isomers were added together to calculate the total coumarates and total ferulates for each species (for individual concentrations of the *cis*- and *trans*-isomers, please refer to **Table 23.** in the appendix). The *cis*- isomers arise from UV light-induced isomerization, formation of the *cis*-isomers is expected to be in forage materials exposed to sunlight

even though plants exclusively synthesize these compounds in their *trans*- forms (Turner et al., 1991).

The total ester-linked ferulate contents varied between species in both growing years (see **Table 7.**). For example, orchardgrass in 2020 had an increase from April to June, but in 2021, the same species produced a decrease in ferulate contents from April to June. Previous studies have observed increased ferulate content under drought conditions (Buanafina & Morris, 2022), however, there was no clear precipitation-related trend seen in this study. Therefore, it can be said that different patterns appear between both harvest year and forage species. This is why it is important to study multiple forage species before making generalizations for the whole forage class. It also is important to have data from multiple harvest years to avoid making too broad of generalizations about seasonal trends.

A trend was seen across both growing seasons in most species for an increase in total coumarates from April to June (see **Table 8.**). The forages tended to have the highest amount of coumarates at the second sampling date in both 2020 and 2021. Tall fescue and Kentucky bluegrass tended to have higher contents of total coumarates compared to the other three species. As mentioned in the literature review, *p*-coumaric acid is often found ester-linked to lignin in grass cell walls. A Pearson's correlation coefficient test was done for total lignin content and total ester-linked coumarates (see **Table 9.**), and there was a moderate correlation with coumarates and lignin in 2020 ($r = .30$, $p < .05$, $n = 67$). There was no correlation in 2021, so it cannot be said that this is a trend that appears reliably every year, but rather one that may be influenced by differences in weather and/or plant age.

Table 7. Total released ester-linked ferulates (μmoles/g) from insoluble cell wall material of cool-season forages

Harvest year	Forage species	April		June		August		October	
2020		mean	SD	mean	SD	mean	SD	mean	SD
	Timothy	19.7[a,b]	6.2	25.1[a]	3.8	13.9[b]	4.3	20.8[a]	3.5
	Tall fescue	23.3[a,b]	2.1	26.0[a]	5.0	16.2[b]	3.5	23.8[a,b]	2.7
	Orchardgrass	35.0[a]	4.0	19.5[b]	4.2	23.5[b]	1.7	22.9[b]	5.2
	KY bluegrass	20.6[a]	6.9	18.7[a]	1.0	15.4[a]	2.6		
	Perennial ryegrass	20.5[a]	7.9	20.8[a]	1.5			14.9[a]	3.6
2021									
	Timothy	25.4[a]	2.5	25.9[a]	3.3	20.6[a]	2.1	20.7[a]	4.8
	Tall fescue	25.5[a]	2.7	26.4[a,b]	1.1	30.6[b]	1.0	27.0[a,b]	2.6
	Orchardgrass	19.4[a]	4.9	24.9[a]	1.9	18.9[a]	3.4	23.6[a]	2.0
	KY bluegrass	22.8[a]	2.6	21.8[a]	1.3				
	Perennial ryegrass	18.5[a]	7.6	21.8[a]	2.2				

Means with different letters in the same row are statistically different between species ($p < 0.05$); means with shared letters in the same row are statistically equivalent
Abbreviations: Standard deviation (SD)

Table 8. Total released ester-linked coumarates (µmoles/g) from insoluble cell wall material of cool-season forages

Harvest year	Forage species	April		June		August		October	
2020		mean	SD	mean	SD	mean	SD	mean	SD
	Timothy	10.3[a,b]	3.1	14.1[a]	3.1	10.2[a,b]	1.6	6.3[b]	1.5
	Tall fescue	13.3[a]	9.0	33.4[b]	1.0	20.3[a]	3.9	23.7[a]	2.7
	Orchardgrass	14.1[a]	1.2	10.3[a]	2.2	10.8[a]	1.0	8.9[a]	1.6
	KY bluegrass	18.9[a]	7.1	22.5[a]	0.6	19.3[a]	3.1		
	Perennial ryegrass	11.0[a,b]	4.3	13.2[a]	0.8			6.7[b]	0.7
2021									
	Timothy	12.0[a]	1.9	16.6[b]	1.9	11.2[b]	1.9	10.9[a]	2.1
	Tall fescue	26.2[a]	2.5	36.9[b]	1.6	34.3[a]	0.6	27.7[a]	2.4
	Orchardgrass	7.1[a]	1.3	13.1[b]	1.6	13.6[b]	1.5	14.7[b]	0.6
	KY bluegrass	24.6[a]	5.0	28.0[a]	1.5				
	Perennial ryegrass	9.0[a]	3.2	12.9[a]	0.9				

Means with different letters in the same row are statistically different between species ($p < 0.05$); means with shared letters in the same row are statistically equivalent
Abbreviations: SD: Standard deviation

Table 9. Pearson's correlation coefficient analysis between total lignin and total ester-linked coumarate monomers for 2020 and 2021 growing seasons

Harvest year			
2020			
		Total coumarates	*Total lignin*
	Total coumarates	**R:** 1 **N:** 67	**R:** 0.3 **Sig (2-tailed):** 0.01 **N:** 67
	Total lignin	**R:** 0.3 **Sig (2-tailed):** 0.01 **N:** 67	**R:** 1 **N:** 67
2021			
		Total coumarates	*Total lignin*
	Total coumarates	**R:** 1 **N:** 61	**R:** 0.02 **Sig (2-tailed):** 0.86 **N:** 61
	Total lignin	**R:** 0.02 **Sig (2-tailed):** 0.86 **N:** 61	**R:** 1 **N:** 61

Correlation is significant at the .01 level (2-tailed).
Abbreviations: N: Sample size, R: Pearson correlation coefficient, and Sig: significance

4.3 Lignin analysis of cell wall material

See section 3.5 in methods.

The acetyl bromide soluble lignin (ABSL) method used in this study was adapted from Barnes and Anderson (2017). Incubation time and temperature were tested to determine ideal conditions that would provide an optimal solubilization of lignin and minimize production of polysaccharide degradation products. The ABSL method from Barnes and Anderson (2017) uses an incubation of 70ºC for 1 hour. Hatfield et al. (1999) recommends a lower incubation temperature and longer incubation time due to the

potential of xylan degradation. High incubation temperatures can cause xylans to degrade and release furfurals. The released furfurals would artificially inflate the amount of ABSL because they are also read at 280 nm. Since grasses have a high amount of xylan, it is likely that the forage species being studied would exhibit inflation in their % ABSL with a higher incubation temperature and shorter time. As can be seen in **Figure 2**, the parameters proposed by Barnes and Anderson (2017) resulted in a larger amount of ABSL, which strongly indicated that xylan was being broken down during incubation and inflating the values. Therefore, it was concluded that the incubation temperature needed to be changed to the more conservative temperature and time combination of 50 ºC for 2 hours.

The lignin content of the insoluble cell wall material of the five forage species was determined by ABSL assay (see **Table 10.**). Differences in lignin composition were observed between sampling dates for various species in both 2020 and 2021. In general, lignin content tended to be lowest during the cool spring sampling period and increased by the warmer second sampling date. Previous literature has seen an increase in lignin as plants mature (Jung 2012). The five different forages analyzed in this study were from older plants, but the harvested tissue represented fresh regrowth since plots were mowed between each harvest date. This shows that any growth obtained in the warmer season will likely have decreased digestibility. There were no clear effects of precipitation or temperature on lignin content. There also was no clear pattern when comparing the 2020 growing season to the 2021 growing season.

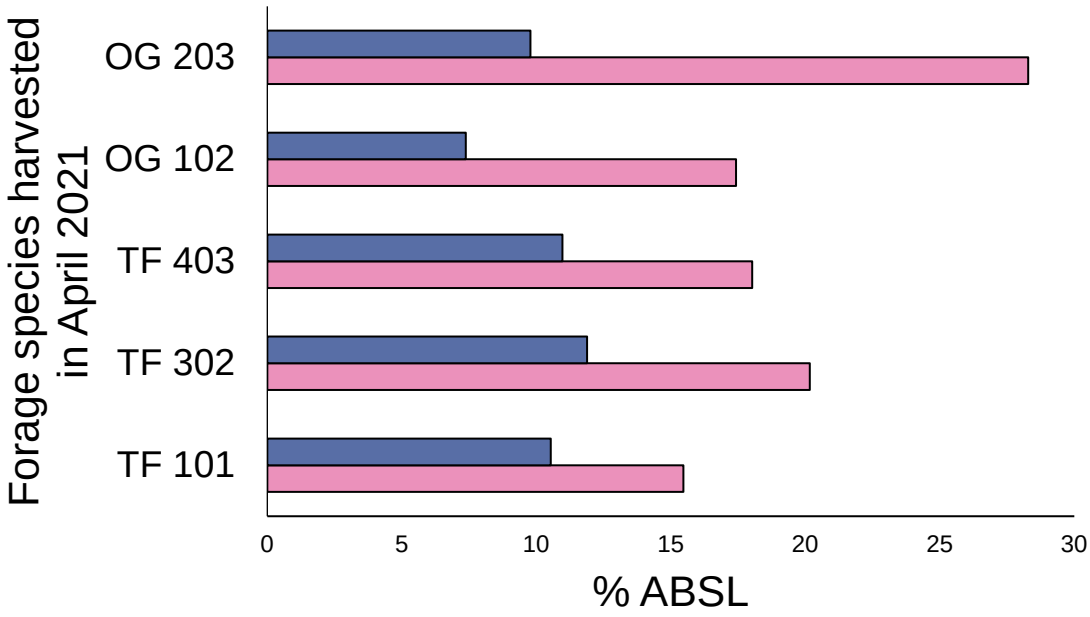

Figure 2. ABSL method incubation time and temperature comparison
Samples were either incubated for 2 hr at 50ºC (blue) or 1 hr at 70ºC (pink).
Abbreviations: ABSL: Acetyl bromide soluble lignin, OG: orchard grass, and TF: tall fescue.

Table 10. % ABSL in insoluble cell wall material of cool-season forages

Harvest year & month	Forage species									
2020	**Timothy**		**Tall fescue**		**Orchard grass**		**KY bluegrass**		**Perennial rye**	
	mean	SD	mean	SD	mean	SD	mean	SD	mean	SD
April	10.2[a]	2.6	6.5[a]	1.0	8.9[a]	1.9	6.8[a]	1.0	8.8[a]	0.4
June	3.4[b]	1.4	18.3[b]	3.0	10.4[a]	2.5	8.6[a]	1.2	11.5[b]	0.6
August	12.4[a]	1.5	13.2[a,b]	2.9	11.5[a]	0.3	11.4[b]	0.9		
October	13.4[a]	2.7	9.4[a]	2.5	11.6[a]	2.0			11.5[b]	0.9
2021										
April	9.1[a]	1.1	7.7[a]	1.5	7.6[a]	1.2	8.0[a]	1.4	7.0[a]	3.8
June	11.7[a]	2.3	11.3[a]	1.9	7.9[a]	1.1	16.4[b]	5.4	8.2[a]	2.5
August	10.2[a]	2.6	12.8[a]	4.7	10.8[a,b]	1.9				
October	8.4[a]	0.8	12.3[a]	1.1	13.7[b]	2.5				

Means with different letters in the same column are statistically different between species ($p < 0.05$); means with shared letters in the same column are statistically equivalent.
Abbreviations: ABSL: Acetyl Bromide Soluble Lignin and SD: standard deviation

4.4 Enzymatic digestion with endoxylanase for production of oligosaccharide profiles in forage materials

A GH10 endoxylanase derived from *Cellvibrio japonicus* (Megazyme) was used to produce AXOS from the forages. This enzyme is an endo-β-1,4 xylanase with a high specific activity for AX. Xylanases from the GH10 family require only two unsubstituted xylose units between branched units (Pollet et al., 2010).

Pure water was used for enzymatic incubation rather than sodium acetate buffer to avoid potential chromatography problems during HPAEC analysis. Ten XOS and AXOS standard compounds (purchased commercially) were selected; please refer to **Figure 6** in the appendix for chemical structures corresponding to standard compounds' abbreviations. Lactose was chosen as the internal standard because it is not native to plant materials. AXOS and XOS in the hydrolysate produced by digestion with *Cellivibrio*

japonicus were quantified using a validated HPAEC-PAD method (Joyce et al., 2023). Samples were analyzed in quadruplicate.

Generation of AXOS fingerprints with an endoxylanase digestion gives a more detailed look at AX structures present in forages over the growing season (see **Figure 3.**). The A/X ratio gave a first glimpse of the degree of substitution along the xylan backbone, but could not give any indication to the pattern of substitution. This method allowed us to compare AX structural fingerprints between species. For example, April 2020 endoxylanase fingerprinting of perennial ryegrass produced a profile that was dominated by 2X and 3X, with smaller amounts of 4X, 5X, and 6X, proving existence of long unsubstituted sections on the xylan backbone for this material. The A/X ratio for the April 2020 perennial ryegrass sample was 0.22, meaning that, if the arabinose units were found as evenly distributed monosubstituents on the xylan backbone, the average maximum length of unsubstituted xylan between substituents would be between DP3 and DP4. The release of longer oligosaccharides proves that the distribution of arabinose units is not even, and that clustering of monosubstituted xylose units or the presence of disubstituted xylose units is likely. A3X, the most commonly released AXOS from GH 10 xylanase was also present. We did not have standard compounds containing disubstituted xylose units, so this structural motif was not included in the profile.

The AXOS screening method can also be used to compare AX structural patterns between species. For example, if we compare the April 2020 perennial rye profile to that of another species in a neighboring plot collected on the same day such as tall fescue (see **Figure 3A.**), a somewhat different fingerprint emerges. No 5X and 6X were able to be quantified for this material and the amount of A3X released was almost the same or

greater as the amount of released 2X and 3X released. Although absolute amounts released are different in timothy, it follows a similar pattern as perennial ryegrass. Orchard grass was similar to tall fescue and did not yield quantifiable amounts of both 5X and 6X.

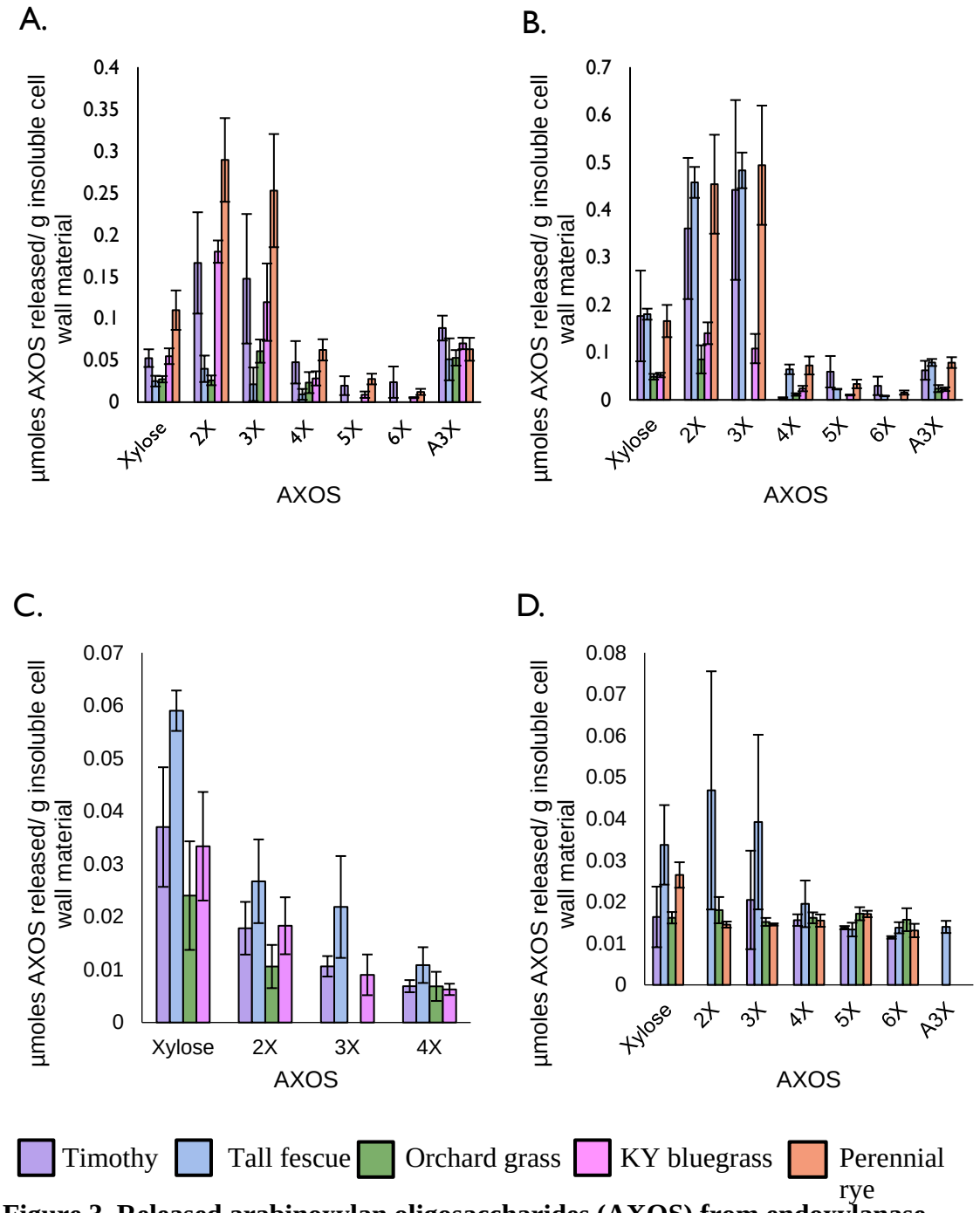

Figure 3. Released arabinoxylan oligosaccharides (AXOS) from endoxylanase digestion of insoluble cell wall material from cool-season forages harvested in 2020
(A.) Harvested April 2020 (B.) Harvested June 2020 (C.) Harvested in August 2020 (D.) Harvested in October 2020. One-way ANOVA and Tukey-Kramer Post Hoc test done for means comparisons can be referenced in section 7.4, tables 24-26. Abbreviations: AXOS: Arabinoxylan oligosaccharide. Please refer to Figure 6 in the appendix for chemical structures corresponding to standard compounds' abbreviations

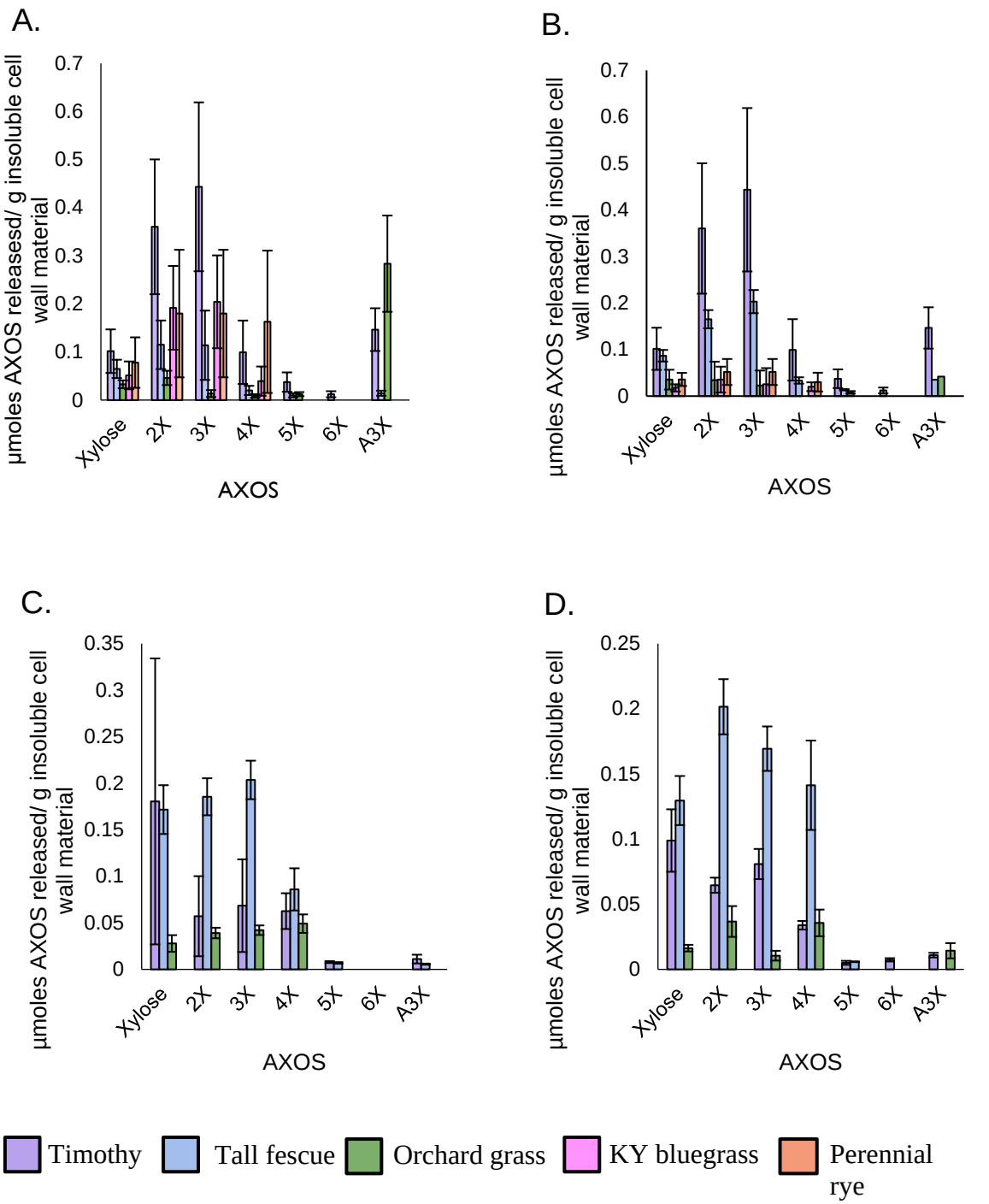

Figure 4. Released arabinoxylan oligosaccharides (AXOS) from endoxylanase digestion

(A.) Harvested April 2021 (B.) Harvested June 2021 (C.) Harvested in August 2021 (D.) Harvested in October 2021. One-way ANOVA and Tukey-Kramer Post Hoc test done for means comparisons can be referenced in section 7.4, tables 24-26.

Abbreviations: AXOS: Arabinoxylan oligosaccharide. Please refer to Figure 6 in the appendix for chemical structures corresponding to standard compounds' abbreviations.

However, we observed some weaknesses in the AXOS screening method when we applied it to samples collected from the later sampling points. For example, to compare the April 2020 to June 2020 samples, we calculated the ratio of released XOS (converted to total milligrams of xylose) to A3X. Given the increased A/X ratio over the growing season, one would expect proportionally more A3X, the smallest substituted AXOS released by GH10 endoxylanases, to be released over the season. However, we observed the opposite trend: proportionally less A3X was released over the season. This indicates that the method may need further optimization for application to later-season samples. Initial optimization steps to consider are expansion of the standard compound set to include additional common examples of substituted AXOS released by endoxylanases and optimization of the endoxylanase incubation conditions.

4.5 Pure culture fermentation

4.5.1 *Monosaccharide analysis after fermentation*

Saeman hydrolysis was done on the pellet material following fermentation to reveal the molar proportions of monosaccharides (see **Table 11.**). The proportions of arabinose and galactose were similar for the samples fermented with *F.succinogenes* and *A. thermocellus*, and the control samples incubated with media only. The proportion of glucose was lower while the proportion of xylose was higher in the bacteria fermented samples compared to the control, indicating a preference for cellulose over AX by the two bacterial species. Additionally, quantification of the monosaccharides on a mg/g basis showed that the arabinose concentration of the bacterial pellets were significantly lower than that of the control (data not shown).

4.5.2 *Endoxylanase digestion with samples after fermentation*

The fermented samples were digested with a GH10 endoxylanase derived from *Cellvibrio japonicus,* and the released oligosaccharides were quantified using the method validated by Joyce et al (2023). Substantial amounts of xylose and 2X were released in the samples fermented with the two bacterial species (see **Figure 5.**), with higher levels of XOS being seen in the fermented samples versus the control. This indicates that fermentation had resulted in a partial stripping of the AX backbone, leaving more sections of unsubstituted xylan accessible to the enzyme. Additionally, the degradation of significant amounts of cellulose in the sample reduced the number of potential sites for hydrogen bonding between cellulose microfibrils and AX, which is known to increase endoxylanase-mediated degradability of AX.

As discussed in section 3.7.1, although the absolute quantity of arabinose was reduced during fermentation, the molar proportions of arabinose stayed the same for the samples fermented with the two bacterial species compared to the control samples. This explains why A3X was still observed in the bacterial fermented samples. However, when the ratio of 2X/A3X was calculated for the fermented samples vs. the control, the ratio was higher for the fermented samples (14.90 and 7.44 for the *F. succinogenes* and *A.thermocellus* samples, respectively, compared to 6.03 for the control). This demonstrates how the AXOS screening method developed and validated by Joyce et al. (2023) enabled the underlying changes in the xylan backbone as a result of fermentation to be seen.

The two bacterial species and the media were incubated with ball milled cellulose to act as a positive control and confirm that no co-eluting peaks were introduced into the HPAEC chromatograms by either the media or bacteria biomass. As expected, these

samples contained large amounts of glucose and cellobiose, the products of cellulose degradation (see **Figure 7.** in the appendix). Injection of standard compounds of these structures proved that the retention times did not conflict with any of the AXOS standard compounds or the internal standard (see **Figure 9.** in the appendix). However, when the baseline of the chromatograms were inspected, quantifiable amounts of xylose, 2X, and 3X were also clearly present. To confirm the origin of these peaks, the ball-milled cellulose was separately incubated with the same endoxylanase and under the same conditions as the AXOS fingerprinting method. Additionally, a control sample of ball-milled cellulose was incubated in water without endoxylanase. Both samples yielded xylose, 2X, and 3X (see **Figure 8.** in the appendix for endoxylanase chromatogram), although the peak areas were clearly increased by endoxylanase digestion. Peak identities were confirmed by spiking the digest with standard compounds. This confirmed that the ball-milled cellulose control contained both xylans and XOS.

Table 11. Molar proportions of monosaccharides released from pellet following fermentation of perennial ryegrass cell wall with pure cultures of fibrolytic bacteria

Bacterial species/control	Ara (%)		Gal (%)		Glu (%)		Xyl (%)		A/X ratio	
	mean	SD	mean	SD	mean	SD	mean	SD	mean	SD
F. succinogenes	6.0[a]	1.2	1.5[a]	0.4	55.2[a]	0.4	37.4[a]	1.4	0.2[a]	0.04
A. thermocellus	5.7[a]	1.7	2.1[a]	0.9	51.4[a]	3.3	40.8[a]	0.8	0.1[a]	0.04
Control	6.4[a]	2.3	1.8[a]	0.8	59.9[b]	1.8	31.9[b]	2.4	0.2[a]	0.09

Means with different letters in the same column are statistically different between species ($p < 0.05$); means with shared letters in the same column are statistically equivalent.
Abbreviations: A. thermocellus: Acetivibrio thermocellus, Ara: arabinose, Gal: galactose, Glu: glucose, F. succinogenes: Fibrobacter succinogenes, and Xyl: xylose

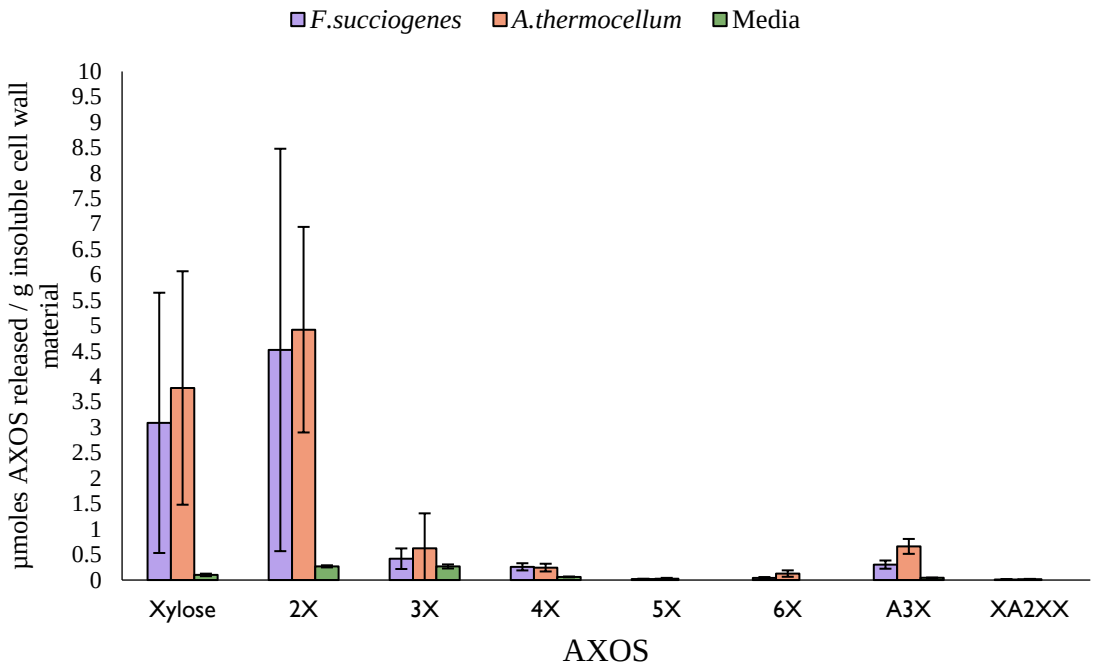

Figure 5. Released arabinoxylan oligosaccharides (AXOS) from endoxylanase digestion of insoluble cell wall material remaining after fermentation with pure fibrolytic bacteria cultures
Abbreviations: A. thermocellus: Acetivibrio thermocellus, AXOS: arabinoxylan oligosaccharide, and F. succinogenes: Fibrobacter succinogenes. Please refer to Figure 6 in the appendix for chemical structures corresponding to standard compounds' abbreviations.

CHAPTER 5. FUTURE RESEARCH DIRECTIONS

There are several other experiments that can be explored to expand on this research. Additional characterization of AX structure would provide a more detailed understanding of cool-season forage cell wall composition. For example, the concentration of dehydrodiferulates, complex oligosaccharide side-chains, and uronic acids could be determined. Further optimization of the AXOS screening method could be performed. There were several peaks in the enzymatic fingerprint that could not be identified or quantified. Expansion of the standard compound set to include additional common examples of substituted AXOS released by endoxylanases would produce a more detailed and informative AX structural fingerprint.

Fermentation could be explored in greater detail by looking at how microbial degradation of forage may differ over the growing season, as well as across harvest years. Also, performing fermentation experiments with mixed rumen fluid would provide more insight into cool season forage degradation by the rumen microbial consortium. Pure culture fermentation alone gives specific insight into the metabolic capabilities of the individual bacteria species. However, it is not representative of the actual rumen environment where multiple species are competing or cooperating to access carbohydrate substrates such as AX.

CHAPTER 6. CONCLUSIONS

In this thesis, the monosaccharide profile, A/X ratio, esterified phenolic acid profile, and lignin content were determined in insoluble cell wall material from five cool-season pasture forages harvested over a four-month period across two growing seasons. The insoluble cell wall material was incubated with an endoxylanase and released AXOS were quantified, generating an AXOS fingerprint at each timepoint. Perennial rye harvested in April of 2020 was fermented with two bacterial species, *Fibrobacter succinogenes* (S85), and *Acetivibrio thermocellus* (27405), as well as a bacteria free control. The monosaccharide profile and oligosaccharide profile of the pellet material were quantified.

Glucose was the dominating monosaccharide in all five species. Arabinose and galactose proportions increased in 2020, but not 2021. There was no overarching trend seen for xylose. The differences in the proportions of arabinose and xylose in the forages revealed the hemicellulosic AX tended to increase over the growing season, and these differences lead to an increase in the rate of backbone substitution. The A/X ratio increased in 2020, but not 2021.

No trends were seen for the total ester-linked ferulates, but there were differences between species. Different patterns were appearing between both harvest year and forage species. This is why it is important to study multiple forage species before making generalizations for the whole forage class. It also is important to have data from multiple harvest years to avoid making too broad of generalizations about seasonal trends.

Contrary to the total ester-linked ferulates in which no clear trends were seen, there were some trends seen for the total ester-linked coumarates. The total coumarates tended to increase from April to June in both growing seasons for. The forages tended to

have the highest amount of coumarates at the second sampling date in both 2020 and 2021. Lignin tended to increase over both growing seasons. The lignin content also tended to be lowest during the cool spring sampling period with an increase at the warmer second sampling date. Lignin content and total coumarates had a moderate correlation in 2020 and no correlation in 2021.

The AXOS screening method allowed for the comparison of AX structural fingerprints between species. When comparing the April 2020 perennial rye profile to that of another species such as tall fescue, a somewhat different fingerprint emerges. Perennial ryegrass produced a profile that was dominated by 2X and 3X, with smaller amounts of 4X, 5X, and 6X. No 5X and 6X were not able to be quantified in tall fescue, and the amount of A3X released was almost the same or greater as the amount of 2X and 3X released. However, some weaknesses were observed in the AXOS screening method when it was applied to samples collected at later sampling points. This indicates that the method may need further optimization for application to later season samples such as, expansion of the standard compound set.

The proportions of arabinose and galactose were similar for the samples fermented with *F.succinogenes* and *A. thermocellus* and the samples in just media. The proportion of glucose was lower while the proportion of xylose was higher in the material remaining after bacterial fermentation compared to the control sample, confirming the preference of these species for cellulose over AX as a growth substrate.

Further structural details of AX changes as a result of bacterial fermentation were revealed by the AXOS fingerprinting method. Proportionally larger amounts of xylose and 2X were released in the samples fermented with the two bacterial species compared

to the control, indicating that bacterial fermentation had generated more sections of exposed, unsubstituted xylan backbone.

CHAPTER 7. APPENDICES

7.1 Appendix A. Additional method information details

7.1.1 *Sample Preparation*

7.1.1.1 Sample collection

1. Forage grasses were planted on September 10th, 2019 in a randomized block design in quadruplicate. Forage grasses were collected in April, June, August, and October of 2020 and 2021 from forage plots managed at the University of Kentucky's Spindletop Farm research station (3250 Iron Works Pike, Lexington, Kentucky). The forage grasses sampled were timothy (*Phleum pretense* L., cultivar "Claire"), perennial ryegrass (*Lolium perenne* L., cultivar "Linn"), Kentucky bluegrass (*Poa pratensis* L., cultivar "Ginger"), orchard grass (*Dactylis glomerata* L., cultivar "Prairie"), and tall fescue (*Schedonorus arundinaceus* (Schreb.) Dumort, cultivar "Cajun II")
2. Cut 5 cm above the base, selectively removing seed heads and dead blades of grass. Collect 500 g (fresh weight) of each species.
3. Record date. Make note of weather conditions prior to forage.
4. Place grass forage into plastic bag, store on ice during transport, and freeze.
5. Transfer forage samples into paper bags and place into freeze dryer for 10 days.
6. Transfer freeze-dried forage samples into plastic Ziploc bags.

7.1.1.2 Milling procedure

1. Weigh lyophilized forage sample prior to milling.
2. Clean out mill. Dust out the mill components, including the 40 mesh (0.5 mm particle size) sieve, funnel, hopper, blades, etc.
3. Use clear packing tape to cover the cracks between the door and the sample.
4. Use clear, plastic garbage bag to form a cover between the flour funnel and receiving container.
5. Once the mill set up is complete, turn on mill.
6. Feed freeze-dried grass sample through hopper, making sure to close hopper lid and hopper shutter with each feeding sample sequence.
7. Wait 1 min during each addition. Tap the flour funnel and mill door to knock sample through the sieve.
8. When done, turn off mill and cut the receiving container free. Have a large empty container available and hold underneath funnel. Slowly open the mill door, brush large sample particles into the new container.
9. Clean mill thoroughly.
10. Mill the leftover particles using a coffee grinder in the lab to 0.5 mm particle size.
11. Weigh milled forage sample on scale and record mass. Record percentage loss.

7.1.1.3 Preparation of water-insoluble plant cell wall materials

1. The method was repeated in quadruplicate for each grass species, or once per plot replicate
2. Suspend 4 g of sample in 50 mL phosphate buffer (0.08 M, pH 6.2) in 250 mL bottle with a screw cap. Add 300 µL Termamyl SC [alpha-amylase, Novozymes]. Incubate for 20 min at 92 ºC, with shaker set at 95 rpm. Swirl flasks every 10 min.

3. Cool sample to room temperature over ice and adjust pH to 4.5 with 0.5 M HCl solution.
4. Add 150 µL AMG 200 [amyloglucosidase, Novozymes] and incubate for 30 min at 60 ºC. Swirl every 5 min.
5. Centrifuge warm solution for 10 min at 5000 rpm.
6. Decant supernatant using pipettes.
7. Wash pellet with 1 × 100 mL and 1 × 50 mL warm water (60º C). Centrifuge after every wash and discard supernatant between washing steps.
8. Wash pellet with 2 × 100 mL and 1 × 50 mL 100% EtOH. Centrifuge after every wash and discard supernatant between washing steps.
9. Wash pellet with 2 × 100 mL and 1 × 50 mL acetone. Centrifuge after every wash and discard supernatant between washing steps. Color should be completely removed from sample, should have the look and consistency of wet sand.
10. Let acetone volatilize in fume hood until there is no discernable odor (48 h). Dry residue overnight in 60º C drying oven.
11. Place in vacuum oven (70º C and 90 mbar) for 48 h.
12. Weigh and store dry samples in desiccator.

7.1.2 *Determination of monosaccharide profile of grass cell wall material*

7.1.2.1 Saeman hydrolysis

1. Weigh in 100 mg of sample in 50 mL glass Pyrex tube (cover threading with Teflon tape, double-check glass rim and threads to confirm that there are no chips), record exact weight. Add 5 glass beads to vial.
2. Add in 1.5 mL 12 M H_2SO_4 and vortex 1 min.
3. Let stand on ice for 30 min, vortex 1 min every 10 min.
4. Let stand at room temperature for 2 h. Vortex 1 min every 30 min.
5. Add 9.75 mL water, vortex 1 min, and then store in drying oven at 100 ºC for 3 h.
6. Filter entire contents in 0.22 µm pore-sized PTFE syringe filter.
7. Use volumetric pipette to transfer exactly 5 mL of filtrate into a new glass tube. Add 40 mL of water. Drop a stir bar in and place on stir plate. Record initial pH. Mix in 3.3 mL 4 M NaOH dropwise until pH ranges between 5-7. If needed, drop additional 4 M NaOH and record exact volume of base added. Bring up to 50 or 100 mL using volumetric flask and DI water.
8. Samples were diluted 1:20 prior to HPAEC-PAD injection.

7.1.2.2 High-performance anion-exchange chromatography (HPAEC-PAD) separation and detection method for monosaccharides

Five-point standard calibration curves were created from monosaccharide standard compounds for two concentration ranges (1-20 µM and 25-125 µM) for the main sugars released in the grass samples by hydrolysis (arabinose, galactose, glucose, and xylose). The resulting chromatographic data was analyzed using the Chromeleon software program (Thermo Scientific Dionex) and peak areas were fitted to quadratic curves in Origin (Pro), (version 2017; OriginLab Corporation, Northampton, MA, USA). The complete analysis was performed in quadruplicate for each grass species.

Table 12. HPAEC-PAD monosaccharide analysis parameters

Columns and dimensions	Guard Column (4 × 50 mm), CarboPac-PA1 (4 × 250 mm)
Company	Thermo-Scientific
Injection volume	25 µL
Flow rate	1.00 mL/min
Column and detector temperature	30 ºC
Detection mode, waveform, electrode	PAD detector, Carbohydrates (Standard Quad), AgCl

Table 13. HPAEC-PAD gradient program for separation of monosaccharides

Gradient Time (min)	Eluent A (Water)	Eluent B (100 mM NaOH)	Eluent C (100 mM NaOH + 0.2 mM NaOAc)
0	90	10	0
1.5	96	4	0
27	96	4	0
37	0	100	0
37.1	0	0	100
47	0	0	100
47.1	0	100	0
57	0	100	0
57.1	90	10	0
67	90	10	0

See 7.2.2 for monosaccharide system eluent preparation.

7.1.3 *Determination of ester-linked phenolic acid content of grass cell wall material*

7.1.3.1 Alkaline hydrolysis

1. Weigh and record 100 mg of de-starched sample into a 50 mL Pyrex glass test tube. Double-check glass rim and threads to confirm that there are no chips. Use open top screw caps and place silica/PTFE faced filters in top of cap.
2. Add 5 mL 2 M NaOH and vortex for 1 min. Use rubber policeman to scrape down sides. Add a small magnetic stir bar.
3. Add 50 µL of 5 mM *trans-o*-coumaric acid as internal standard (end concentration will be 250 µM)

4. Set samples in a 500 mL beaker on stir plate and turn on stirring to 75% capacity. Visually check if material is properly mixing.
5. Cover entire system with aluminum foil and let sit for at least 18 h with constant stirring.
6. Acidify samples with 2 mL of 12 N HCl. Check if samples are <pH 2.
7. Extract with diethyl ether. Add volume of ether (6 mL, 5 mL, 5 mL) to sample, invert 3 times, release pressure, and centrifuge at 2000 rpm for 10 min. Pipette off top ether layer into separate glass vial. Combine all extractions for each sample (samples analyzed in quadruplicate).
8. Dry ether extracts under N_2 stream (should take at least 1 h until completely dry) in fume hood using Microvap manifold (Organomation).
9. Dissolve residues in 1 mL MeOH/H_2O (50/50 v/v) and store at 4º C covered in aluminum foil. Samples are diluted 1:10 prior to run on HPLC (use 0.25 mM *ortho*-coumaric acid solution, prepared in 50/50 v/v MeOH/H_2O, as diluting liquid).

7.1.3.2 Conversion of trans-*ferulic/*trans-p-*coumaric acid to* cis-*ferulic/*cis-p-*coumaric acid*

1. Prepare separate 5 mM stock solution (50 mL) of *trans*-ferulic and *trans-p*-coumaric acid.
2. Pipette 10 mL of solution into 50 mL volumetric flask.
3. Clamp two UV lamps to buret stands. Place flasks under lamps and create an aluminum foil cage (reflective side facing inward) around the flasks and lamp. Create a cardboard partition to cover the aluminum foil. Let sit for a minimum of 24 h.
4. Bring flask up to volume with 50/50 v/v MeOH/H_2O. The theoretical end concentration of untransformed *trans*-ferulic/ *trans-p*-coumaric acid would be 1 mM.
5. Run transformed stocks on HPLC with parameters listed in **Table 6-3.**
6. Make a 6-point calibration curve for *trans*-ferulic and *trans-p*-coumaric from a 5 mM stock (concentration range 0.1 mM-1 mM). Calculate the concentration of the remaining *trans*-ferulic and *trans-p*-coumaric acid based on the calibration curve in the light-exposed. The *cis* concentration is 1 mM minus (calculated remaining *trans*). Calculate the proportion of conversion (*cis* concentration/*trans* concentration).

7.1.3.3 High-performance liquid chromatography (HPLC) separation and detection method for hydroxycinnamic acid

Phenolic acid compounds were detected at 325 nm and quantified with linear, equidistant, 6-point internal calibration curves (*trans*-ferulic and *trans*-*p*-coumaric acid, 100-1000 µM; *cis*-ferulic and *cis*-*p*-coumaric acid, 10-100 µM), using *ortho*-coumaric as the internal standard (250 µM)

Table 14. High-performance liquid chromatography (HPLC) parameters for separation and detection of hydroxycinnamic acidsT

Column and dimensions	5 µM Phenyl-Hexyl (Luna), 100 Å, LC Column 250 × 4.6 mm
Company	Phenomenex
Injection volume	10 µL
Flow rate	1.1 mL/min
Column and detector temperature	45 ºC
Detection mode, waveform, electrode	DAD detector, quantification wavelength 325 nm, slit width 1.2 nm

Table 15. High-performance liquid chromatography (HPLC) gradient program for separation of hydroxycinnamic acids

Gradient time (min)	**Eluent A (1 mM TFA in H_2O)**	**Eluent B [90/10 (Acetonitrile): (1 mM TFA in 50/50 v/v MeOH/H_2O)]**
0	88	12
13	88	12
23	85	15
28	85	15
33	84	16
27	34	66
42	34	66
43	88	12
53	88	12

See section 8.4 for HPLC eluent preparation

7.1.4 *Lignin analysis*

7.1.4.1 Acetyl Bromide Soluble Lignin

This method is based off the protocol from (Barnes & Anderson, 2017). It is highly recommended to read this reference before performing this assay.

Purpose: This assay includes the preparation of alcohol insoluble residue (AIR) from biomass samples and the consequent solubilization of lignin so that it can be analyzed with a spectrophotometer.

Important Safety Reminders: *Pay attention to any hazard precautions included throughout this protocol. Gloves should be worn for all steps, but some steps (especially when working with acetyl bromide) require more PPE and use of the fume hood.*

Part I: Alcohol Insoluble Residue (AIR) Preparation and Destarching

1. Weight about 50 mg of finely ground tissue into a 2 mL centrifuge tube. Record the weight.
2. Add 1 mL of 70% ethanol to the tube; vortex; centrifuge the tube at max setting for one minute to pellet the residue (repeat the centrifugation if a pellet was not formed). Pour off the supernatant gently without disturbing the pellet. (All additions and removals of reagents should be performed in the fume hood.)
3. Add 1 mL of 1:1 chloroform: methanol to the tube; vortex re-suspend pellet; centrifuge and remove supernatant as in the previous step.
4. Add 1 mL of acetone; vortex, and centrifuge to remove supernatant. Allow material suspended in residual acetone to air dry in the fume hood **overnight** with caps open. Once dry, the remaining material is AIR.
5. Destarch AIR: add 1 mL 90% DMSO to pellet; vortex and allow to shake **overnight** on a platform rocker (50 rpm or more at the highest angle for mixing[3]). The next day, centrifuge and remove supernatant as previously done.
6. Wash once in 1 mL 90% DMSO; vortex, and centrifuge to remove supernatant as previously done.
7. Wash six times with 1 mL of 70% Ethanol; vortex, and centrifuge to remove supernatant each time.
8. Add 1 mL of acetone; vortex, and centrifuge to remove the supernatant. Allow material suspended in residual acetone to air dry **overnight** in fume hood. The material remaining is destarched AIR.

Part II: Acetyl Bromide Soluble Lignin Determination

1. Weigh about 5 mg of destarched AIR and put into one glass screw cap vial; record exact mass.
2. (Wear a lab coat, gloves, and protective eye gear when working with acetyl bromide in the hood. From this point, only glass pipettes and glassware should be used—no plastic.) In a fume hood, prep 25% acetyl bromide by diluting with glacial acetic acid (Note: Acetyl Bromide has a strong adverse reaction with water). While prepping the acetyl bromide, the water bath should be turned on to preheat to 50 ºC.
3. To each glass tube with destarched AIR, gently add 1 mL of 25% acetyl bromide. Also add 1 mL of 25% acetyl bromide to an empty tube to serve as a blank. Gently swirl the tubes to suspend the fibers.

4. Put all samples in the water bath at 50 ºC for 2 h. Gently swirl every 10 min.
5. Remove the samples after 2 h and put samples on ice to cool them. While on ice, add 5 mL of glacial acetic acid to stop the reaction. Ensure the caps are closed and vortex the samples thoroughly in the fume hood.
6. Allow residual AIR to settle to bottom of the tube for at least 1 h to overnight.
7. Once settled, transfer 300 µL from the top of the acetyl bromide solution to a glass open-top tube while avoiding re-suspending any residual AIR (if the residue is disturbed and the solution is not clear, set sample aside and re-do at the end). Add 400 µL of 1.5 N NaOH to the tube. Then, add 300 µL of 0.5 M freshly made hydroxylamine hydrochloride (diluted with DI water). Finally, dilute mixture with 1 mL of glacial acetic acid. Gently pipette up and down to mix solution thoroughly. Then, add 800 µL of solution to a clean quartz cuvette. Read the sample on the spectrophotometer at 280 nm. Record absorbance.
8. Between samples, rinse the inside of cuvette with glacial acetic acid and wipe the sides with a Kim wipe and 70% ethanol. Use a new glass open-top tube to mix the next sample.
9. After reading all the samples, clean cuvette and dispose of all waste in the proper containers. Be careful when cleaning sample tubes with residual acetyl bromide to "flood" the samples with lots of water continuously for about 15-30 S each to avoid hazard. Continue to wear PPE while cleaning glassware.

7.1.5 *Oligosaccharide creation and analysis*

7.1.5.1 Xylanase digestion of insoluble cell wall material

1. Pipette 50 µL of enzyme solution (E-XYACJ, CAS Number: 9025-57-4, GH 10, *Megazyme*) into 1950 µL of DI water to make working enzyme solution (12.5 U/mL).

2. Weigh out 30 mg of sample (repeat in quadruplicate) into 2 mL Eppendorf tube with screw cap.

3. Add 24 µL of working enzyme solution and 1176 µL of DI water in sample tube.

4. Set dry bath to 12 h at 60 ºC at 600 rpm.

5. Put samples in boiling water bath at 95 ºC for 15 min to deactivate enzymes.

6. Centrifuge for 14000 rpm for 10 min. Pipette off 500 µL supernatant and dilute with 1 mL of DI water.

7. Filter through 0.22 µm PTFE filter.

8. Add 25 µL of 10 µM lactose stock (internal standard) to 475 µL of xylanase digested sample (liquid fraction).

8. Freeze all fractions in -20 ºC.

7.1.5.2 High-performance anion-exchange chromatography (HPAEC-PAD) separation and detection method for arabinoxylan oligosaccharides

Table 16. . HPAEC-PAD analysis parameters for arabinoxylan oligosaccharides

Columns and dimensions	CarboPac PA-200 (3 x 250 mm), Guard Column (3 x 50 mm)
Company	Thermo-Scientific
Injection volume	25 µL
Flow rate	1.00 mL/min
Column and detector temperature	30ºC
Detection mode, waveform, electrode	PAD detector, Carbohydrates (Standard Quad), AgCl

Table 17. Oligosaccharide HPAEC-PAD separation gradient

Gradient Time (min)	Eluent A (Water)	Eluent B (100 mM NaOH)	Eluent C (100 mM NaOH + 1 M NaOAc)
0	75	25	0
10	0	100	0
20	0	100	0
24.5	0	97.5	2.5
29.5	0	97.5	2.5
55	0	83.4	16.6
55.1	0	0	100
75.1	0	0	100
75.2	0	100	0
95.2	0	100	0
95.3	75	25	0
105	75	25	0

7.1.6 *Pure culture fermentation*

7.1.6.1 Sample preparation

1. Weigh out 125 mg to 150 mg of isolated insoluble cell wall material (repeat in quadruplicate) into 18 x 150 mm Balch tubes.

7.1.6.2 Pure culture fermentation

Notes: Bacteria used for pure culture fermentation were *Fibrobacter succinogenes* (S85) and *Acetivibrio thermocellus* (27405). The cultures were grown on cellulose paper and then transferred to ball mill cellulose for the controls. *Fibrobacter succinogenes* (S85) was grown in celluloytic defined media (PC + VFA + PAA) and *Acetivibrio thermocellus* (27405) was grown in thermophile medium (T. medium). Media preparation procedure found in section 8.6.

1. Add 6.25 mL of media to 125 mg samples and 7.5 mL of media to 150 mg samples (should equal out to be 2% substrate and 10% inoculum).

2. Incubate samples for 5 days. Place samples containing *Acetivibrio thermocellus* in water bath at 63ºC and 100 rpm. Place samples containing *Fibrobacter succinogenes* or the controls (just media & sample) in a water bath at 39ºC and 100 rpm.
3. After incubation, collect 3 mL of supernatant.
4. Transfer remaining amount of sample into 15 mL plastic conical tubes. Add 6-7.5 mL of water to Balch tubes to collect any remaining sample. The final volume in the 15 mL centrifuge tube should be 10 mL.
5. Centrifuge for 10 min at 15,000 G and collect remaining supernatant.
6. Add 5 mL of water, vortex, and centrifuge at 15,000 G for 10 min (repeat 2 times). Collect water after each centrifuge.
7. Freeze all fractions in -20ºC freezer. Sample pellet needs to be frozen for min 24 h.
8. Dry sample pellet in freeze-dryer.

7.2 Appendix B. Equipment, enzyme, and reagents

Table 18. Analytical instruments

Instrument	Description	Manufacturer
HPAEC-PAD	Thermo Scientific Dionex ICS-5000+ system, Dionex ICS-5000 dual pump, AS-AP autosampler, ICS-5000 DC electrochemical detector	Thermo Scientific
HPLC	Shimadzu SIL-20AC autosampler, Two LC-20AT pumps, DGU-20A3 degasser, SPD-M20A P detector	Shimadzu

Table 19. Enzymes

Enzyme name	Activity	Source	Manufacturer
AMG 300®	Amyloglucosidase, 300 AGU/mL	*Aspergillus niger*	Novozymes
E-XYACJ, CAS Number: 9025-57-4	Xylanase, GH 10, 500 U/mL	*Cellvibrio japonicas*	Megazymes
Termamyl SC®	Alpha-amylase, 120 KNU/g	Genetically modified *Bacicillus* (proprietary)	Novozymes

Table 20. Chemicals and reagents

Chemical name, purity	CAS number	Manufacturer
Acetic acid, Glacial	64-19-7	VWR Chemicals
Acetone, 99.5%	67-64-1	VWR Chemicals
Acetonitrile, HPLC grade, 99.8%	666-52-4	EMD Millipore
Acetyl bromide, 99%	506-96-7	Sigma-Aldrich
Chloroform, ≥ 99.9%	67-66-3	VWR Chemicals
Dimethyl sulfoxide (DMSO), ≥ 99.9%	67-68-5	VWR Chemicals
D-Galactose, ≥ 99%	59-23-4	Acros Organics, Fisher Scientific
D (+)- Glucose anhydrous, ≥ 99%	50-99-7	Acros Organics, Fisher Scientific
Diethyl ether, 99%	60-29-7	JT Baker
D-Lactose monohydrate, ≥ 99.5%	63-42-3	Sigma-Aldrich
Ethanol, 99.5%	64-17-5	VWR Chemicals
Hydrochloric acid (HCl) 6N solution	7647-01-0	Fisher Chemical
Hydroxylamine hydrochloride, 98%	5470-11-1	Sigma-Aldrich
L-Arabinose, 99%	5328-37-0	VWR Life Science
Methanol, HPLC gradient grade, 100%	67-56-1	VWR Chemicals
Sodium acetate anhydrous (NaOAc), 99%	127-09-3	OmniPOur, EMD Millipore
Sodium hydroxide (NaOH) 50% w/w solution	1310-73-2	Fisher Chemical
Sodium hydroxide (NaOH), 97%	1310-73-2	VWR Chemicals
Sodium phosphate dibasic anhydrous (Na_2HPO_4), 98%	7558-79-2	VWR Chemicals
Sodium phosphate monobasic monohydrate ($NaH_2PO_4 \times H_2O$), 98%	7558-79-4	VWR Chemicals
Sulfuric acid (H_2SO_4), 95-98%	7664-21-5	VWR Chemicals
Trifluoroacetic acid (TFA), 99.9%	76-05-1	VWR Life Sciences

7.2.1 *Phosphate buffer preparation*

1. Add 500 mL DI water to a 1-L volumetric flask. Dissolve 12.48 g sodium phosphate monobasic dihydrate ($NaH_2PO_4 \cdot 2H_2O$) in volumetric flask thoroughly (use stir bar if necessary) and bring up to volume.
2. Add 500 mL DI water to 1-L volumetric flask. Dissolve 11.36 g sodium phosphate dibasic (Na_2HPO_4) in volumetric flask thoroughly (use stir bar and plate if necessary) and bring up to volume.
3. Combine 815 mL NaH_2PO_4 x H_2O solution and 195 mL Na_2HPO_4. Adjust solution to pH 6.2. Label phosphate buffer "0.08 M, pH 6.2" with the date of preparation. Store solution in fridge. Solution is good for up to 3 weeks.

7.2.2 *Monosaccharide gradient preparation*

7.2.2.1 Eluent B preparation (100 mM NaOH)
1. Measure 2 L of deionized water. Remove 10.4 mL of water.
2. Degas water by gently sparging with nitrogen gas for 15 min.
3. Remove nitrogen gas line from eluent bottle.
5. Add 10.4 mL of concentrated NaOH solution (commercially prepared, 50% w/w).
    a. Do not mix or agitate NaOH solution bottle in this process. Take NaOH from middle of container to minimize contamination with carbonate on the surface layers of the solution. Tightly cap NaOH solution bottle immediately afterwards.
6. Tilt back and forth gently to ensure thorough mixing of eluent with minimal air incorporation.
7. Screw cap back on eluent bottle and open helium gas line to bottle to maintain a helium headspace.

7.2.2.2 Eluent C preparation (200 mM NaOAc + 100 mM NaOH)
1. Measure 1 L of deionized water. Remove 5.2 mL of water.
2. Measure 32.8 g of NaOAc and add to 1 L of water. Gently mix bottle. Slowly add in the 2nd 1 L of water into eluent bottle. Add in a stir bar and mix to ensure there are no particles in the bottle.
3. Degas solution by gently sparging with nitrogen gas for 15 min.
4. Remove nitrogen gas line from eluent bottle.
5. Add 5.2 mL of concentrated NaOH solution (commercially prepared, 50% w/w)
    a. Do not mix or agitate NaOH solution bottle in this process. Take NaOH from middle of container to minimize contamination with carbonate on the surface layers of the solution. Tightly cap NaOH solution bottle immediately afterwards.
6. Tilt back and forth gently to ensure thorough mixing of eluent with minimal air incorporation.
7. Screw cap back on eluent bottle and open helium gas line to bottle to maintain a helium headspace over the eluent.

7.2.3 *Gradient preparation for hydroxycinnamic acid separation*

7.2.3.1 Eluent A preparation for HPLC separation of hydroxycinnamic acids
1. Put slightly less than 1 L of DI water in volumetric flask.
2. Add 0.08 mL of trifluoroacetic acid (TFA) to flask for a concentration of 1 mM TFA and bring to volume with water

3. Mix thoroughly and transfer eluent to HPLC glass bottles. Label bottle with date of preparation.
4. Degas by gently sparging with nitrogen gas for 15 minutes.

7.2.3.2 Eluent B preparation for HPLC separation of hydroxycinnamic acids

1. Separately measure 500 mL of DI water and 500 mL of MeOH and combine in a glass HPLC eluent bottle. Do not bring up to volume.
2. Add 0.08 mL of TFA into 50/50 v/v H_2O/MeOH bottle and mix thoroughly.
3. In a new empty glass HPLC eluent bottle, add 900 mL of acetonitrile and 100 mL of 1 mM TFA prepared in 50/50 (v/v) H_2O/MeOH from step 2. Combine thoroughly. Label bottle with date of preparation.
4. Degas by sparging with nitrogen gas for 15 minutes.

7.2.4 *Oligosaccharide gradient preparation (HPAEC)*

7.2.4.1 Eluent B preparation (100 mM NaOH)

1. Put 2L of DI water in eluent bottle.
2. Degas water by sparging with nitrogen gas for 15 min.
3. Add 10.4 mL of concentrated NaOH solution (commercially prepared, 50% w/w)
    a. Do not mix or agitate NaOH solution bottle in this process. Take NaOH from middle of container to minimize contamination with carbonate on the surface layers of the solution. Tightly cap NaOH solution bottle immediately afterwards.

4. Gently mix the solution by rocking back and forth (avoid agitation to minimize incorporation of air).
5. Reattach helium gas line to bottle to maintain a helium headspace over the eluent.

7.2.4.2 Eluent C preparation (1 M NaOAc + 100 mM NaOH)

1. Put ~400 mL of DI water in a 1-L volumetric flask. Place a stir bar in volumetric flask and place on stir plate. Set stir plate to #5 setting.
2. Add 82 g NaOAc into volumetric flask. Add 200 mL of DI water. Wait until powder is fully dissolved then bring flask up to volume. Remove stir bar and readjust and bring to volume again.
3. Transfer contents to eluent bottle.
4. Repeat steps 1-3 until eluent bottle has 2 liters.
5. Degas eluent bottle by gently sparging with nitrogen gas for 15 minutes.
6. Add 10.4 mL of concentrated NaOH solution (commercially prepared, 50% w/w)
    a. Do not mix or agitate NaOH solution bottle in this process. Take NaOH from middle of container to minimize contamination with carbonate on the surface layers of the solution. Tightly cap NaOH solution bottle immediately afterwards.
7. Seal the eluent bottle with a normal cap. Total volume of eluent should be 2.0104 L.
8. Gently mix the eluent solution by rocking back and forth (avoid agitation to minimize incorporation of air).
9. Reattach eluent line cap on eluent bottle. Turn on flow of helium gas to bottle to maintain a helium headspace over the eluent.

7.2.5 *Media preparation*

7.2.5.1 Cellulolytic defined media (PC + VFA + PAA)

Table 21. Composition of cellulolytic defined

Salt A	40 mL
Salt B	40 mL
Yeast extract	0.50 g
Trypticase	1 g
H_2O	900 mL
VFA solution	3.1 mL
Cysteine hydrochloride	0.6 g
Phenylacetate	1 g
Resazurin stock	1 mL

Procedure:
1. Starting pH is 3.3, adjust pH to 6.5 with 10% NaOH.
2. Autoclave for 15 minutes.
3. Cool to room temperature under CO_2.
4. Add 4 g Na_2CO_3.

7.2.5.2 Thermophile medium (T medium)

Table 22. Composition of thermophile medium

Salt T1	50 mL
Salt T2	50 mL
Yeast extract	2 g
Vitamins	10 mL
Modified metals	5 mL
Cysteine	0.5 g
Resazurin stock	1 mL
H_2O	850 mL

Procedure:
1. Adjust pH to 6.7 with 10% NaOH.
2. Autoclave for 10 minutes to degas medium. Ensure autoclave is set to slow exhaust.
3. Bubble with CO_2 until medium cools to room temperature.
4. Anaerobically add 50 mL of 8% Na_2CO_3 (4g/L) to the medium.
5. Anaerobically transfer the medium to tubes (9 mL) or to serum bottles (80 mL).
6. Autoclave 20 minutes.

7.3 Appendix C. Additional data figures and tables

Table 23. Ester-linked trans-ferulic (FA), cis-ferulic (FA), trans-p-coumaric (pCA), and cis-p-coumaric (pCA) acid insoluble cell wall material of cool-season pasture grasses

Harvest year	Forage species							
2020		**April**		**June**		**August**		**October**	
		mean	SD	mean	SD	mean	SD	mean	SD
	Timothy								
	Trans-FA	13.2	6.7	19.7	3.3	10.9	3.3	14.7	2.4
	Cis-FA	3.5	2.3	5.4	0.5	3.0	1.0	6.1	1.1
	*Trans-p*CA	9.3	3.1	12.3	2.7	7.0	1.6	5.1	1.2
	*Cis-p*CA	1.6	1.2	1.9	0.3	1.1	0.3	1.1	0.3
	Tall fescue								
	Trans-FA	19.0	1.8	22.0	0.9	12.7	2.8	18.6	1.9
	Cis-FA	4.2	0.8	6.3	0.5	3.5	0.8	5.3	1.0
	*Trans-p*CA	17.7	1.9	26.7	1.0	16.2	3.2	23.6	2.7
	*Cis-p*CA	0.03	0.007	6.7	0.3	4.1	0.8	0.1	0.01
	Orchardgrass								
	Trans-FA	28.2	2.8	14.9	3.1	18.4	1.2	17.1	4.1
	Cis-FA	6.9	1.2	4.6	1.1	5.1	0.5	5.8	1.1
	*Trans-p*CA	11.7	0.9	8.4	1.8	10.8	1.0	8.5	2.3
	*Cis-p*CA	2.4	0.4	1.9	0.5	0.02	0.004	1.0	1.0
	Kentucky bluegrass								
	Trans-FA	15.4	5.3	13.5	0.9	11.2	1.9		
	Cis-FA	5.2	1.7	5.2	0.2	4.3	0.8		
	*Trans-p*CA	14.7	5.7	17.2	0.4	14.8	2.3		
	*Cis-p*CA	4.2	1.5	5.2	0.3	4.5	0.8		
	Perennial ryegrass								
	Trans-FA	16.9	6.8	14.7	1.2			10.7	2.2
	Cis-FA	4.1	1.6	6.1	0.3			4.2	1.4
	*Trans-p*CA	9.3	3.6	10.1	0.7			5.1	0.5
	*Cis-p*CA	1.8	0.6	3.1	0.1			1.6	0.2
2021									
	Timothy								
	Trans-FA	24.1	2.2	23.1	2.7	16.3	1.2	16.3	3.4
	Cis-FA	1.3	0.4	2.7	0.7	4.4	0.9	4.4	1.3
	*Trans-p*CA	11.1	2.0	15.1	1.5	9.9	1.5	9.8	1.7
	*Cis-p*CA	0.9	0.2	1.6	0.4	1.3	0.4	1.1	0.4

Tall fescue								
Trans-FA	23.4	2.8	22.6	1.1	24.7	1.1	22.0	2.1
Cis-FA	2.1	0.5	3.8	0.3	5.9	0.6	5.0	0.6
*Trans-p*CA	22.5	2.0	30.2	1.4	28.8	1.1	23.2	2.1
Cis-pCA	3.7	0.5	6.7	0.6	5.6	0.5	4.5	0.5
Orchardgrass								
Trans-FA	17.3	4.5	21.0	1.7	18.9	3.4	19.8	1.6
Cis-FA	2.2	0.7	3.3	0.4	4.9	1.4	3.8	0.4
*Trans-p*CA	6.4	1.1	11.1	1.1	11.8	1.1	12.7	0.5
*Cis-p*CA	0.7	0.2	1.9	0.3	1.7	0.4	2.0	0.2
Kentucky bluegrass								
Trans-FA	20.4	2.6	18.4	0.8				
Cis-FA	2.4	0.3	3.4	0.5				
*Trans-p*CA	20.1	4.2	22.9	0.8				
*Cis-p*CA	4.5	0.8	5.0	0.8				
Perennial ryegrass								
Trans-FA	16.8	6.6	18.5	2.2				
Cis-FA	1.7	1.0	3.3	0.9				
*Trans-p*CA	7.9	2.5	10.5	0.9				
*Cis-p*CA	1.2	0.7	2.4	0.6				

Abbreviations: SD: Standard deviation

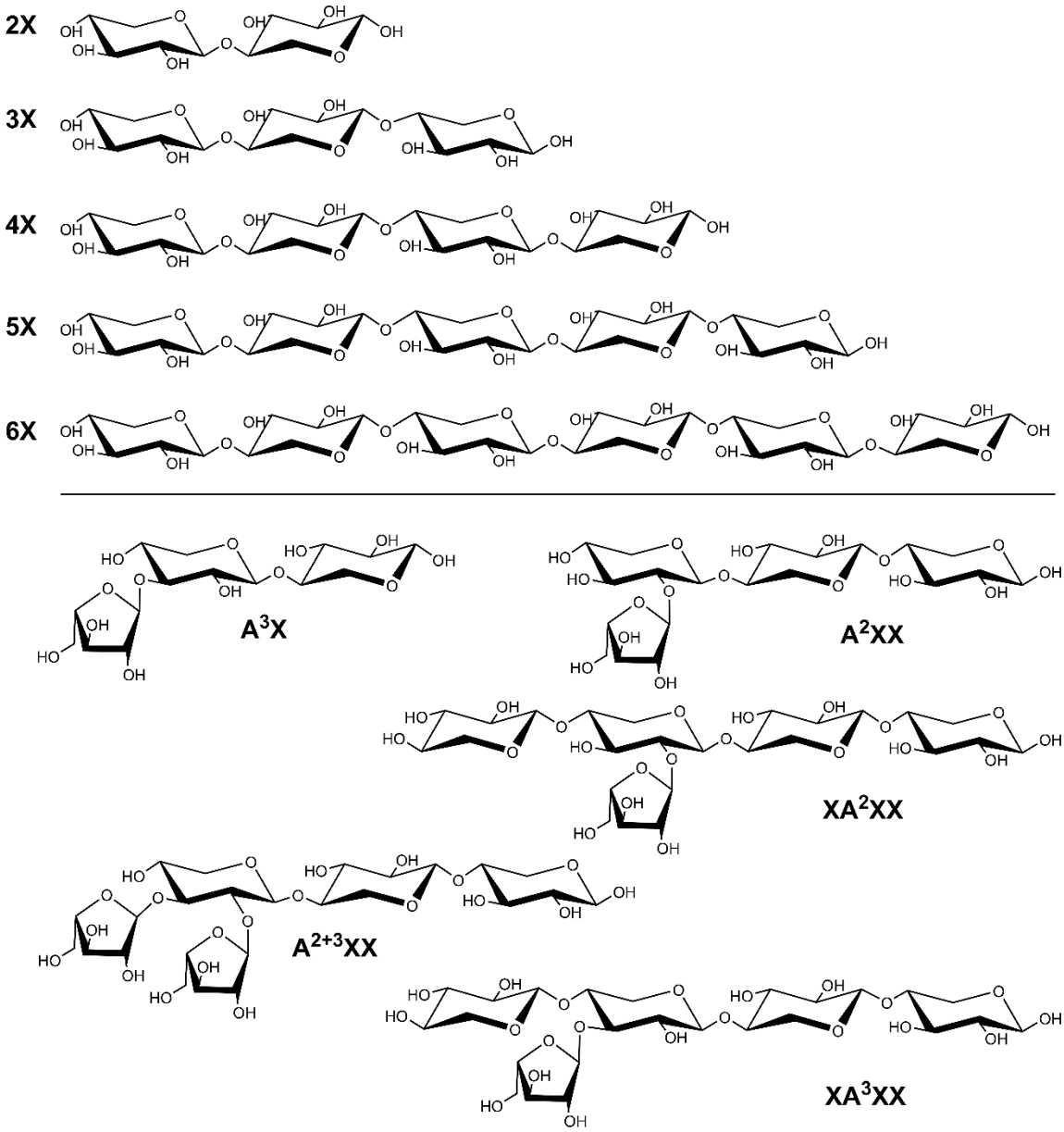

Figure 6. Chemical structures and abbreviations of oligosaccharide standard compounds utilized in study
Figure modified from Joyce et al. (2023).

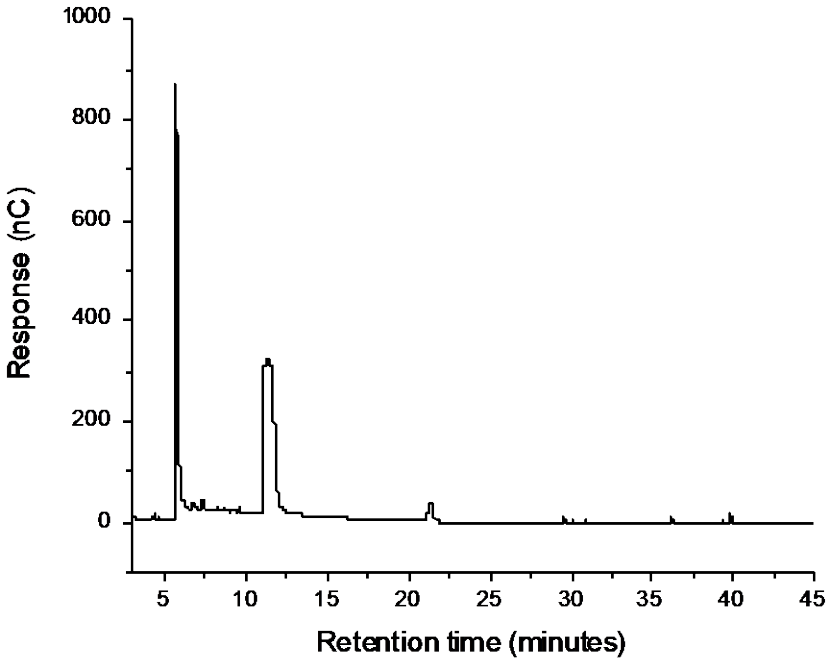

Figure 7. HPAEC chromatogram for A. thermocellus incubated with ball milled cellulose

Pellet remaining after fermentation was subjected to endoxylanase digestion, and the supernatant produced after enzymatic hydrolysis was injected into the HPAEC

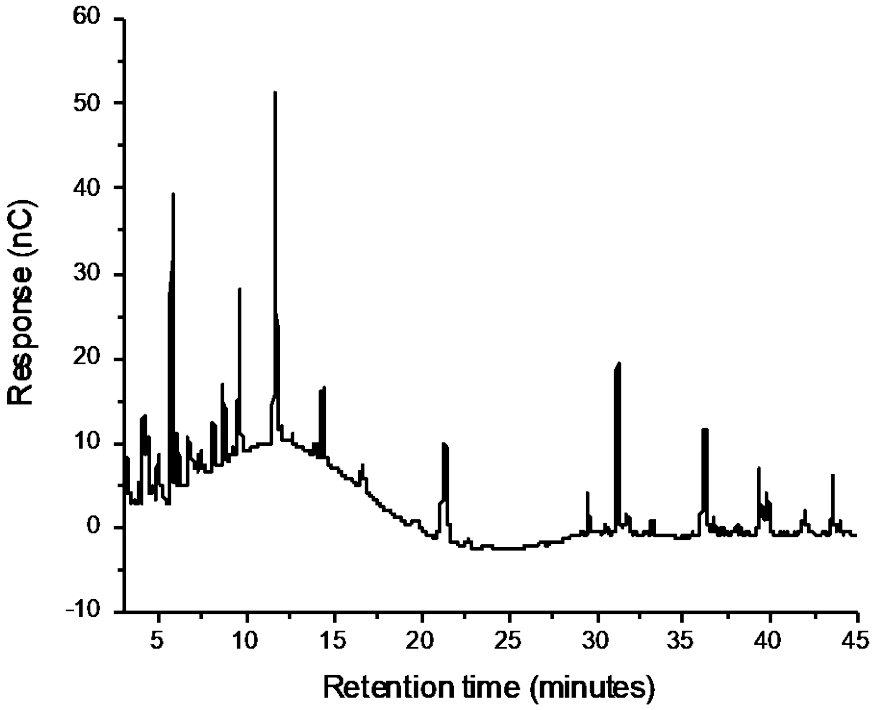

Figure 8. HPAEC chromatogram of enzymatic hydrolysate generated by incubation of ball milled cellulose sample with endoxylanase

A.

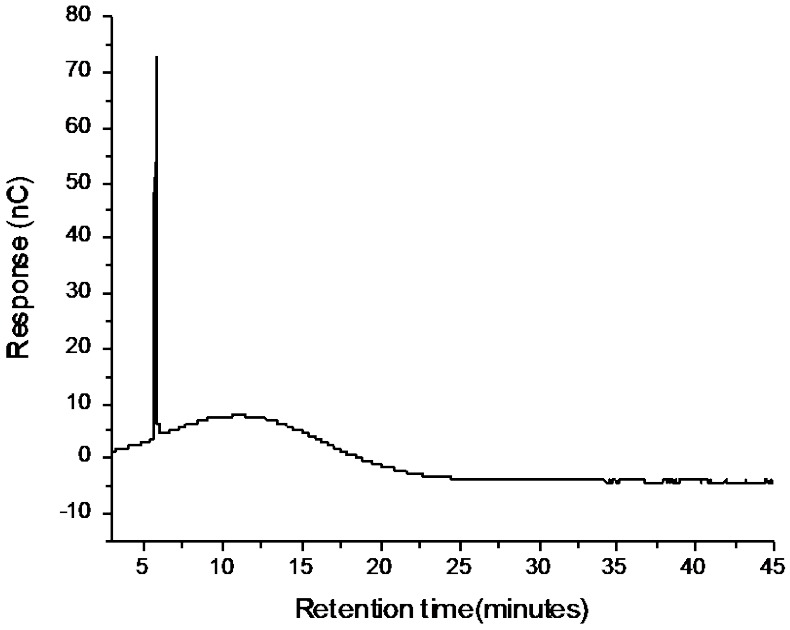

B.

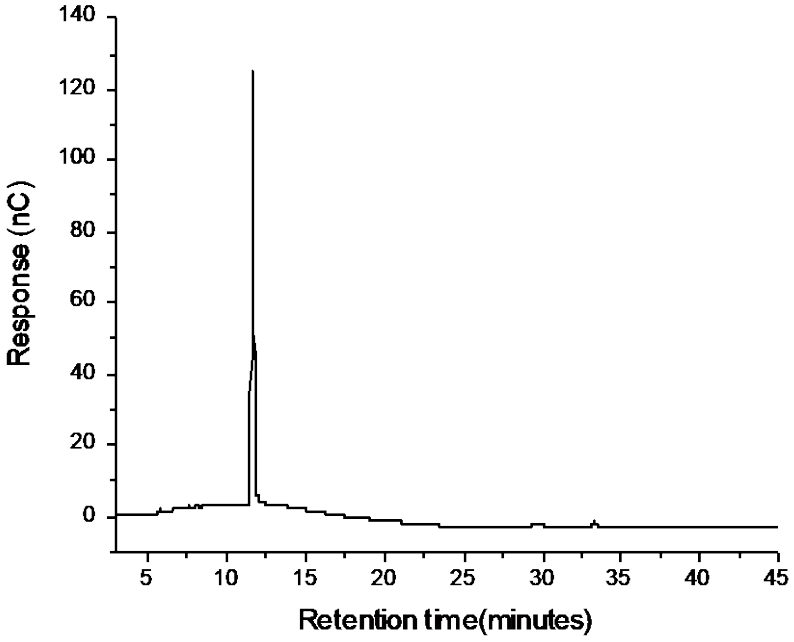

Figure 9. HPAEC chromatograms depicting the retention times of glucose and cellobiose when injected using the same chromatographic conditions as the AXO quantification method

(A). 10 µM glucose stock solution and (B). 25 µM cellobiose stock solution

7.4 Appendix D. Statistical results

Table 24. Statistical results (p-values) arising from means comparisons for individual oligosaccharides in different harvest months using Tukey-Kramer Post Hoc test

Year	Species	Month	Xyl	2X	3X	4X	5X	6X	A3X
2020						*p*-value			
	Tim								
		April *June*	0.05	0.1	0.03	0.17	0.16	0.91	0.08
		April *August*	0.98	0.24	0.41	0.6	0.96	0.73	-
		April *October*	0.81	0.38	0.45	0.75	-	-	-
		June *August*	0.03	0.01	0.004	0.02	0.16	0.5	-
		June *October*	0.01	0.02	0.004	0.03	-	-	-
		August *October*	0.95	1	1	1	-	-	-
	TF								
		April *June*	<.001	<.001	<.001	<.001	-	-	.06
		April *August*	.001	.89	1	1	-	-	.02
		April *October*	.58	.98	.78	.27	-	-	-
		June *August*	<.001	<.001	<.001	<.001	<.001	-	<.001
		June *October*	<.001	<.001	<.001	<.001	-	-	-
		August *October*	.01	.65	.75	.34	-	-	-
	OG								
		April *June*	.008	.001	.03	.27	-	-	.01
		April *August*	.88	.43	.03	.14	-	-	-
		April *October*	.18	.87	-	.68	-	-	-
		June *August*	.003	<.001	.82	.99	-	-	-
		June *October*	<.001	<.001	-	.94	-	-	-

	August							
	October	.45	.9	-	.82	-	-	-
KY								
	April							
	June	.92	.33	.89	.59	.93	-	<.001
	April							
	August	.02	<.001	.003	.002	-	-	-
	June							
	August	.05	<.001	.01	.01	-	-	-
PR								
	April							
	June	.02	.03	.02	.63	.47	.49	.14
	April							
	October	.002	.002	.05	.02	.16	.95	-
	June							
	October	<.001	<.001	.001	.01	.03	.71	-
2021								
Tim								
	April							
	June	.82	.01	.01	.24	.15	.26	.001
	April							
	August	.61	.003	.002	.56	.13	.46	<.001
	April							
	October	1	.01	.01	.27	.1	-	.002
	June							
	August	.21	.92	.96	.9	.98	.94	.99
	June							
	October	.91	.98	.99	.99	.93	-	.99
	August							
	October	.72	1	1	.83	1	-	1
TF								
	April							
	June	.43	.15	.04	.81	.16	-	<.001
	April							
	August	<.001	.03	.04	.004	.29	-	.01
	April							
	October	.003	.009	.26	<.001	.1	-	
	June							
	August	<.001	.79	1	.02	.01	-	<.001
	June							
	October	.04	.38	.65	<.001	.002	-	-
	August							
	October	.05	.88	.64	.01	.9	-	-

OG								
	April June	.99	.88	.89	.98	.14	-	<.001
	April August	.94	.97	.2	<.001	-	-	<.001
	April October	.28	.93	1	.01	-	-	-
	June August	.82	.99	.44	.02	-	-	.79
	June October	.18	1	.75	.13	-	-	-
	August October	.57	1	.1	.22	-	-	-
KY								
	April June	.11	.03	.03	.35	-	-	-
PR								
	April June	.17	.11	.13	-	-	-	-

-, absent or unquantifiable amount found.
Month column provides the variables that are being compared.
Abbreviations: AXOS: Arabinoxylan oligosaccharide, KY: Kentucky bluegrass, OG: orchard grass, PR: perennial ryegrass, TF: tall fescue, Tim: timothy, and Xyl: xylose. Please refer to Figure 6 in the appendix for chemical structures corresponding to standard compounds' abbreviations.

Table 25. Statistical results (p-values) arising from means comparisons for individual oligosaccharides in different species using Tukey-Kramer Post Hoc test

Year	Month	Species	Xyl	2X	3X	4X	5X	6X	A3X
2020						*p*-value			
	April								
		Tim TF	.14	.01	.03	.03	-	-	.03
		Tim OG	.15	.002	.15	.21	-	-	.02
		Tim KY	1	1	.92	.41	.29	-	.37
		Tim PR	<.001	.01	.92	.65	.38	.27	.14
		TF OG	1	.99	.78	.69	-	-	1
		TF KY	.07	.01	.08	.42	-	-	.47
		TF PR	<.001	<.001	.08	.002	-	-	.8
		OG KY	.07	.001	.39	.99	-	-	.49
		OG PR	<.001	<.001	.39	.01	-	-	.84
		KY PR	<.001	.003	1	.03	.03	-	.97
	June								
		Tim TF	1	.56	.99	.22	.06	-	.35
		Tim OG	.03	.01	.04	.01	-	-	.01
		Tim KY	.04	.04	.03	.02	.02	-	.01
		Tim PR	1	.6	.97	.36	.24	.2	.36
		TF OG	.03	<.001	.02	.28	-	-	<.001
		TF KY	.03	.002	.01	.52	.82	-	<.001
		TF PR	.99	1	1	1	.81	-	1
		OG KY	1	.92	.93	.99	-	-	1
		OG PR	.05	<.001	.02	.17	-	-	<.001

	KY PR	.06	.003	.01	.35	.37	-	<.001
August								
	Tim TF	.04	.25	.14	.49	-	-	-
	Tim OG	.31	.41	.84	.78	-	-	-
	Tim KY	.95	1	.98	1	-	-	-
	TF OG	.001	.01	.6	.94	-	-	-
	TF KY	.01	.23	.06	.31	-	-	-
	OG KY	.51	.3	.66	.6	-	-	-
October								
	Tim TF	.01	.78	.25	.57	-	-	-
	Tim OG	1	.89	-	1	-	-	-
	Tim PR	.18	.8	.98	1	.01	.27	-
	TF OG	.02	.29	-	.64	-	-	-
	TF PR	.43	.22	.25	.63	-	-	-
	OG PR	.22	1	-	1	-	-	-
2021								
April								
	Tim TF	.58	.03	.02	.05	.03	-	.04
	Tim OG	.09	.01	.004	.02	.04	-	.03
	Tim KY	.3	.19	.1	.19	-	-	-
	Tim PR	.87	..14	.05	.38	-	-	-
	TF OG	.7	.83	.78	.99	.96	-	<.001
	TF KY	.98	.77	.8	.94	-	-	-
	TF PR	.98	.86	.97	.85	-	-	-

	OG KY	.94	.24	.25	.76	-	-	-
	OG PR	.39	.31	.46	.63	-	-	-
	KY PR	.82	1	.98	1	-	-	-
June	*Tim TF*	.05	.06	.01	.67	.82	-	.13
	Tim OG	.89	.21	.05	.17	.12	-	.07
	Tim KY	.27	.29	.09	.13	-	-	-
	Tim PR	.91	.54	.08	-	-	-	-
	TF OG	.01	<.001	<.001	.43	.03	-	.83
	TF KY	.002	.002	<.001	.5	-	-	-
	TF PR	.01	.003	<.001	-	-	-	-
	OG KY	.71	1	1	.93	-	-	-
	OG PR	1	.95	1	-	-	-	-
	KY PR	.69	.97	1	-	-	-	-
August	*Tim TF*	.99	<.001	<.001	.25	.32	-	.23
	Tim OG	.09	.64	.49	.64	-	-	.57
	TF OG	.11	<.001	<.001	.08	-	-	.05
October	*Tim TF*	.12	<.001	<.001	.003	.31	-	-
	Tim OG	.001	.18	<.001	1	-	-	-
	TF OG	<.001	<.001	<.001	<.001	-	-	-

-, absent or unquantifiable amount found

Species column provides the variables being compared

Abbreviations: KY: Kentucky bluegrass, OG: orchardgrass, PR: perennial ryegrass, TF: tall fescue, Tim: timothy), and Xyl: xylose. Please refer to Figure 6 in the appendix for chemical structures corresponding to standard compounds' abbreviations.

Table 26. Statistical results (p-values) arising from means comparisons for AXOS fingerprints of individual species using Tukey-Kramer Post Hoc test

Harvest year	Harvest month	Oligo	Timothy	Tall fescue	Orchard grass	KY bluegrass	Perennial ryegrass
2020					*p*-value		
	April						
		Xyl 2X	.03	.81	1	<.001	<.001
		Xyl 3X	.1	1	.002	.01	<.001
		Xyl 4X	1	.77	.98	.6	.45
		Xyl 5X	.94	-	-	.12	.03
		Xyl 6X	.97	-	-	-	.01
		Xyl A3X	.88	.36	.02	.94	.47
		2X 3X	1	.66	.001	.1	.72
		2X 4X	.02	.23	.99	<.001	<.001
		2X 5X	.01	-	-	<.001	<.001
		2X 6X	.01	-	-	-	<.001
		2X A3X	.18	.91	.01	<.001	<.001
		3X 4X	.07	.89	<.001	<.001	<.001
		3X 5X	.01	-	-	<.001	<.001
		3X 6X	.02	-	-	-	<.001
		3X A3X	.46	.25	.78	.07	<.001
		4X 5X	.97	-	-	.88	.77
		4X 6X	.99	-	-	-	.39
		4X A3X	.8	.07	.01	.18	1
		5X 6X	1	-	-	-	.99

	5X A3X	.29	-	-	.02	.75
	6X A3X	.36	-	-	-	.37
June						
	Xyl 2X	.18	<.001	.11	<.001	<.001
	Xyl 3X	.02	<.001	.22	.01	<.001
	Xyl 4X	.96	<.001	.1	.32	.4
	Xyl 5X	.56	<.001	-	.06	.09
	Xyl 6X	.31	-	-	-	.04
	Xyl A3X	.59	<.001	.37	.28	.48
	2X 3X	.93	.57	.01	.21	.97
	2X 4X	.03	<.001	.003	<.001	<.001
	2X 5X	.01	<.001	-	<.001	<.001
	2X 6X	.002	-	-	-	<.001
	2X A3X	.01	<.001	.01	<.001	<.001
	3X 4X	.003	<.001	1	<.001	<.001
	3X 5X	<.001	<.001	-	<.001	<.001
	3X 6X	<.001	-	-	-	<.001
	3X A3X	<.001	<.001	.86	<.001	<.001
	4X 5X	.97	.11	-	.9	.97
	4X 6X	.83	-	-	-	.86
	4X A3X	.98	.93	.86	1	1
	5X 6X	1	-	-	-	1
	5X A3X	1	.02	-	.93	.95

	6X A3X	1	-	-	-	.79
August						
	Xyl 2X	.02	<.001	.08	.02	-
	Xyl 3X	.002	<.001	.47	<.001	-
	Xyl 4X	<.001	<.001	.05	<.001	-
	Xyl 5X	.01	<.001	-	-	-
	Xyl 6X	.01	-	-	-	-
	Xyl A3X	-	<.001	-	-	-
	2X 3X	.63	.83	.87	.2	-
	2X 4X	.24	.01	1	.07	-
	2X 5X	.96	.06	-	-	-
	2X 6X	.8	-	-	-	-
	2X A3X	-	.05	-	-	-
	3X 4X	.96	.12	.77	.92	-
	3X 5X	.99	.41	-	-	-
	3X 6X	1	-	-	-	-
	3X A3X	-	.41	-	-	-
	4X 5X	.76	.99	-	-	-
	4X 6X	.94	-	-	-	-
	4X A3X	-	.97	-	-	-
	5X 6X	1	-	-	-	-
	5X A3X	-	1	-	-	-
	6X A3X	-	-	-	-	-

October						
	Xyl 2X	.47	.75	.9	-	<.001
	Xyl 3X	1	.97	.99	-	<.001
	Xyl 4X	1	.71	1	-	<.001
	Xyl 5X	-	-	1	-	<.001
	Xyl 6X	-	-	1	-	<.001
	Xyl A3X	-	-	-	-	-
	2X 3X	.57	.94	.72	-	1
	2X 4X	.47	.22	.81	-	.99
	2X 5X	-	-	1	-	.57
	2X 6X	-	-	.79	-	.93
	2X A3X	-	-	-	-	-
	3X 4X	1	.47	1	-	1
	3X 5X	-	-	.94	-	.68
	3X 6X	-	-	1	-	.95
	3X A3X	-	-	-	-	-
	4X 5X	-	-	.97	-	.93
	4X 6X	-	-	1	-	.72
	4X A3X	-	-	-	-	-
	5X 6X	-	-	.98	-	.17
	5X A3X	-	-	-	-	-
	6X A3X	-	-	-	-	-

2021						
April						
	Xyl 2X	.01	.43	1	.06	.47
	Xyl 3X	<.001	.45	.99	.04	.59
	Xyl 4X	1	.54	.96	.99	-
	Xyl 5X	.93	.33	.98	-	-
	Xyl 6X	.8	-	-	-	-
	Xyl A3X	.99	.42	<.001	-	-
	2X 3X	.88	1	.91	.99	.98
	2X 4X	.01	.02	.81	.04	-
	2X 5X	.001	.01	.86	-	-
	2X 6X	.001	-	-	-	-
	2X A3X	.05	.01	<.001	-	-
	3X 4X	<.001	.02	1	.02	-
	3X 5X	<.001	.01	1	-	-
	3X 6X	<.001	-	-	-	-
	3X A3X	.003	.01	<.001	-	-
	4X 5X	.94	1	1	-	-
	4X 6X	.82	-	-	-	-
	4X A3X	.98	1	<.001	-	-
	5X 6X	1	-	-	-	-
	5X A3X	.54	1	<.001	-	-
	6X A3X	.4	-	-	-	-

June	*Xyl 2X*	.56	<.001	1	.78	.57
	Xyl 3X	.31	<.001	.99	.98	.92
	Xyl 4X	1	<.001	.97	1	-
	Xyl 5X	.83	<.001	.71	-	-
	Xyl 6X	.7	-	-	-	-
	Xyl A3X	.76	<.001	1	-	-
	2X 3X	1	.02	.99	.95	.37
	2X 4X	.48	<.001	.97	.84	-
	2X 5X	.09	<.001	.74	-	-
	2X 6X	.06	-	-	-	-
	2X A3X	.1	<.001	1	-	-
	3X 4X	.25	<.001	1	.99	-
	3X 5X	.04	<.001	.97	-	-
	3X 6X	.02	-	-	-	-
	3X A3X	.05	<.001	.91	-	-
	4X 5X	.89	>39	1	-	-
	4X 6X	.78	-	-	-	-
	4X A3X	.82	1	.91	-	-
	5X 6X	1	-	-	-	-
	5X A3X	1	.31	.51	-	-
	6X A3X	1	-	-	-	-
August	*Xyl 2X*	.23	.89	.24	-	-

	Xyl 3X	.33	.19	.1	-	-
	Xyl 4X	.27	<.001	.01	-	-
	Xyl 5X	.13	<.001	-	-	-
	Xyl 6X	.13	-	-	-	-
	Xyl A3X	.04	<.001	.12	-	-
	2X 3X	1	>73	.98	-	-
	2X 4X	1	<.001	.41	-	-
	2X 5X	.98	<.001	-	-	-
	2X 6X	.98	-	-	-	-
	2X A3X	.96	<.001	.002	-	-
	3X 4X	1	<.001	.71	-	-
	3X 5X	.95	<.001	-	-	-
	3X 6X	.95	-	-	-	-
	3X A3X	.9	<.001	<.001	-	-
	4X 5X	.97	<.001	-	-	-
	4X 6X	.97	-	-	-	-
	4X A3X	.94	<.001	<.001	-	-
	5X 6X	1	-	-	-	-
	5X A3X	1	1	-	-	-
	6X A3X	1	-	-	-	-
October						
	Xyl 2X	.14	.002	.02	-	-
	Xyl 3X	.63	.11	.75	-	-

	Xyl 4X	.01	.93	.03	-	-
	Xyl 5X	.001	<.001	-	-	-
	Xyl 6X	-	-	-	-	-
	Xyl A3X	.002	-	-	-	-
	2X 3X	.7	.26	.003	-	-
	2X 4X	.2	.01	1	-	-
	2X 5X	.01	<.001	-	-	-
	2X 6X	-	-	-	-	-
	2X A3X	.02	-	-	-	-
	3X 4X	.04	.38	.004	-	-
	3X 5X	.004	<.001	-	-	-
	3X 6X	-	-	-	-	-
	3X A3X	.01	-	-	-	-
	4X 5X	.24	<.001	-	-	-
	4X 6X	-	-	-	-	-
	4X A3X	.42	-	-	-	-
	5X 6X	-	-	-	-	-
	5X A3X	.99	-	-	-	-
	6X A3X	-	-	-	-	-

-, absent or unquantifiable amount
Oligo column provides the variables that are being compared
Abbreviations: AXOS: Arabinoxylan oligosaccharide. Oligo: oligosaccharide
Please refer to Figure 6 in the appendix for chemical structures corresponding to standard compounds' abbreviations.

REFERENCES

AACCI. (2001). The Definition of Dietary Fiber. *Cereal Foods World*, *46*, 112-126.

Albersheim, P., Darvill, A., Roberts, K., Sederoff, R., & Staehelin, A. (2010a). Biochemistry of the Cell Wall Molecules. In *Plant Cell Walls*. Garland Science

Albersheim, P., Darvill, A., Roberts, K., Sederoff, R., & Staehelin, A. (2010b). The Structural Polysaccharides of the Cell Wall and How They are Studied. In *Plant Cell Walls* (pp. 24). Garland Science

Allerdings, E., Ralph, J., Steinhart, H., & Bunzel, M. (2006). Isolation and Structural Identification of Complex Feruloylated Heteroxylan Side-Chains From Maize Bran. *Phytochemistry*, *67*(12), 1276-1286.

Åman, P. (1993). Composition and Structure of Cell Wall Polysaccharides in Forages. In *Forage Cell Wall Structure and Digestibility* (pp. 183-199).

Ana, L. M., Rogelio, S., Xose Carlos, S., & Rosa Ana, M. (2022). Cell Wall Composition Impacts Structural Characteristics of the Stems and Thereby the Biomass Yield. *Journal of Agricultural and Food Chemistry*, *70*(10), 3136-3141.

Andersson, A. A. M., Lampi, A.-M., Nyström, L., Piironen, V., Li, L., Ward, J. L., Gebruers, K., Courtin, C. M., Delcour, J. A., Boros, D., Fraś, A., Dynkowska, W., Rakszegi, M., Bedő, Z., Shewry, P. R., & Åman, P. (2008). Phytochemical and Dietary Fiber Components in Barley Varieties in the HEALTHGRAIN Diversity Screen. *Journal of Agricultural and Food Chemistry*, *56*(21), 9767-9776.

Appeldoorn, M. M., de Waard, P., Kabel, M. A., Gruppen, H., & Schols, H. A. (2013). Enzyme Resistant Feruloylated Xylooligomer Analogues From Thermochemically Treated Corn Fiber Contain Large Side Chains, Ethyl Glycosides and Novel Sites of Acetylation. *Carbohydrate Research*, *381*, 33-42.

Badhan, A., Low, K. E., Jones, D. R., Xing, X., Milani, M. R. M., Polo, R. O., Klassen, L., Venketachalam, S., Hahn, M. G., Abbott, D. W., & McAllister, T. A. (2022). Mechanistic Insights Into the Digestion of Complex Dietary Fibre by the Rumen Microbiota Using Combinatorial High-Resolution Glycomics and Transcriptomic Analyses. *Computational and Structural Biotechnology Journal*, *20*, 148-164.

Barberousse, H., Roiseux, O., Robert, C., Paquot, M., Deroanne, C., & Blecker, C. (2008). Analytical Methodologies for Quantification of Ferulic Acid and its Oligomers. *Journal of the Science of Food and Agriculture*, *88*(9), 1494-1511.

Barnes, W. J., & Anderson, C. T. (2017). Acetyl Bromide Soluble Lignin (ABSL) Assay for Total Lignin Quantification from Plant Biomass. *Bio-protocol*, *7*(5), 1-11.

Beaugrand, J., Chambat, G., Wong, V. W. K., Goubet, F., Rémond, C., Paës, G., Benamrouche, S., Debeire, P., O'Donohue, M., & Chabbert, B. (2004). Impact and Efficiency of GH10 and GH11 Thermostable Endoxylanases on Wheat Bran

and Alkali-Extractable Arabinoxylans. *Carbohydrate Research, 339*(15), 2529-2540.

Beaugrand, J., Crônier, D., Debeire, P., & Chabbert, B. (2004). Arabinoxylan and hydroxycinnamate content of wheat bran in relation to endoxylanase susceptibility. *Journal of Cereal Science, 40*, 223-230.

Boerjan, W., Ralph, J., & Baucher, M. (2003). Lignin Biosynthesis. *Annual Review of Plant Biology, 54*, 519-546.

Buanafina, M. M. (2009). Feruloylation in Grasses: Current and Future Perspectives. *Molecular Plant, 2*(5), 861-872.

Buanafina, M. M., & Morris, P. (2022). The Impact of Cell Wall Feruloylation on Plant Growth, Responses to Environmental Stress, Plant Pathogens and Cell Wall Degradability. *Agronomy, 12*(8).

Bunzel, M., Allerdings, E., Sinwell, V., Ralph, J., & Steinhart, H. (2002). Cell Wall Hydroxycinnamates in Wild Rice (*Zizania aquatica L.*) Insoluble Dietary Fibre. *European Food Research and Technology, 214*(6), 482-488.

Bunzel, M., Ralph, J., Marita, J. M., Hatfield, R. D., & Steinhart, H. (2001). Diferulates as Structural Components in Soluble and Insoluble Cereal Dietary Fibre. *Journal of the Science of Food and Agriculture, 81*(7), 653-660.

Casler, M. D. (2001). Breeding Forage Crops for Increased Nutrititonal Value. *Advances in Agronomy, 71*, 51-107.

Casler, M. D., & Jung, H.-J. G. (2006). Relationships of Fibre, Lignin, and Phenolics to *in Vitro* Fibre Digestibility in Three Perennial Grasses. *Animal Feed Science and Technology, 125*(1-2), 151-161.

Chandelia, M., Garg, A., Lutjohann, D., Von Bergmann, K., Grundy, S. M., & Brinkley, L. (2000). Beneficial Effects of High Dietary Fiber Intake in Patients with Type 2 Diabetes Mellitus. *New England Journal of Medicine, 342*, 1392-1398.

Chateigner-Boutin, A. L., Ordaz-Ortiz, J. J., Alvarado, C., Bouchet, B., Durand, S., Verhertbruggen, Y., Barriere, Y., & Saulnier, L. (2016). Developing Pericarp of Maize: A Model to Study Arabinoxylan Synthesis and Feruloylation. *Frontiers in plant science, 7*, 1476.

Cloetens, L., Broekaert, W. F., Delaedt, Y., Ollevier, F., Courtin, C. M., Delcour, J. A., Rutgeerts, P., & Verbeke, K. (2010). Tolerance of Arabinoxylan-Oligosaccharides and Their Prebiotic Activity in Healthy Subjects: A Randomised, Placebo-Controlled Cross-Over Study. *British Journal of Nutrition, 103*(5), 703-713.

Corradini, C., Cavazza, A., & Bignardi, C. (2012). High-Performance Anion-Exchange Chromatography Coupled with Pulsed Electrochemical Detection as a Powerful

Tool to Evaluate Carbohydrates of Food Interest: Principles and Applications. *International Journal of Carbohydrate Chemistry*, *2012*, 1-13.

Deleu, L. J., Lemmens, E., Redant, L., & Delcour, J. A. (2020). The Major Constituents of Rye (*Secale cereale* L.) Flour and Their Role in the Production of Rye Bread, a Food Product to Which a Multitude of Health Aspects are Ascribed. *Cereal Chemistry*, *97*(4), 739-754.

Dhakarey, R., Raorane, M. L., Treumann, A., Peethambaran, P. K., Schendel, R. R., Sahi, V. P., Hause, B., Bunzel, M., Henry, A., Kohli, A., & Riemann, M. (2017). Physiological and Proteomic Analysis of the Rice Mutant cpm2 Suggests a Negative Regulatory Role of Jasmonic Acid in Drought Tolerance. *Frontiers in plant science*, *8*, 1903.

Dobberstein, D., & Bunzel, M. (2010). Separation and Detection of Cell Wall-Bound Ferulic Acid Dehydrodimers and Dehydrotrimers in Cereals and Other Plant Materials by Reversed Phase High-Performance Liquid Chromatography With Ultraviolet Detection. *Journal of Agricultural and Food Chemistry*, *58*(16), 8927-8935.

Dodd, D., Mackie, R. I., & Cann, I. K. (2011). Xylan Degradation, a Metabolic Property Shared by Rumen and Human Colonic *Bacteroidetes*. *Molecular Microbiology*, *79*(2), 292-304.

Duan, P., Kaser, S. J., Lyczakowski, J. J., Phyo, P., Tryfona, T., Dupree, P., & Hong, M. (2021). Xylan Structure and Dynamics in Native *Brachypodium* Grass Cell Walls Investigated by Solid-State NMR Spectroscopy. *ACS Omega*, *6*(23), 15460-15471.

Ehlke, N. J., & Undersander, D. J. (1990). *Cool Season Grasses*.

Fanuel, M., Grélard, F., Foucat, L., Alvarado, C., Arnaud, B., Chateigner-Boutin, A.-L., Saulnier, L., Legland, D., & Rogniaux, H. (2022). Spatial Correlation of Water Distribution and Fine Structure of Arabinoxylans in the Developing Wheat Grain. *Carbohydrate Polymers*, *294*, 119738.

Feng, G., Flanagan, B. M., Mikkelsen, D., Williams, B. A., Yu, W., Gilbert, R. G., & Gidley, M. J. (2018). Mechanisms of Utilisation of Arabinoxylans by a Porcine Faecal Inoculum: Competition and Co-Operation. *Scientific Reports*, *8*(1), 4546.

Fukushima, R. S., Kerley, M. S., Ramos, M. H., & Kallenbach, R. L. (2021). The Acetyl Bromide Lignin Method Accurately Quantitates Lignin in Forage. *Animal Feed Science and Technology*, *276*.

Fukushima, R. S., Kerley, M. S., Ramos, M. H., Porter, J. H., & Kallenbach, R. L. (2015). Comparison of Acetyl Bromide Lignin with Acid Detergent Lignin and Klason Lignin and Correlation With *in Vitro* Forage Degradability. *Animal Feed Science and Technology*, *201*, 25-37.

Gebruers, K., Dornez, E., Boros, D., Fras, A., Dynkowska, W., Bedo, Z., Rakszegi, M., Delcour, J. A., & Courtin, C. M. (2008). Variation in the Content of Dietary Fiber and Components Thereof Wheats in the HEALTHGRAIN Diversity Screen. *Journal of Agricultural and Food Chemistry, 56,* 9740–9749.

Gibson, G. R., Hutkins, R., Sanders, M. E., Prescott, S. L., Reimer, R. A., Salminen, S. J., Scott, K., Stanton, C., Swanson, K. S., Cani, P. D., Verbeke, K., & Reid, G. (2017). Expert Consensus Document: The International Scientific Association for Probiotics and Prebiotics (ISAPP) Consensus Statement on the Definition and Scope of Prebiotics. *Nature Reviews: Gastroenterology & Hepatology*, *14*(8), 491-502.

Gordon, A. H., Lomax, J. A., Dalgarno, K., & Chesson, A. (1985). Preparation and Composition of Mesophyll, Epidermis and Fibre Cell Walls from Leaves of Perennial Ryegrass (*Lolium perenne*) and Italian Ryegrass (*Lolium multiflorum*). *Journal of the Science of Food and Agriculture, 36*(7), 509-519.

Grabber, J. H. (2005). How do Lignin Composition, Structure, and Cross-Linking affect Degradability? A Review of Cell Wall Model Studies. *Crop science*, *45*(3), 820-831.

Grabber, J. H. (2019). Relationships between Cell Wall Digestibility and Lignin Content as Influenced by Lignin Type and Analysis Method. *Journal of Crop Science*, *59*(3), 1122-1132.

Grabber, J. H., Hatfield, R., Ralph, J., Zon, J., & Amrhein, N. (1995). Ferulate Cross-Linking in Cell Walls Isolated from Maize Cell Suspensions. *Phytochemistry*, *40*, 1077-1082.

Grabber, J. H., Hatfield, R. D., & Ralph, J. (1998). Diferulate Cross-Links Impede Enzymatic Degradation of Non-Lignified Maize Walls. *Journal of the Science of Food and Agriculture, 77*, 193-200.

Grabber, J. H., Mertens, D. R., Kim, H., Funk, C., Lu, F., & Ralph, J. (2009). Cell Wall Fermentation Kinetics are Impacted more by Lignin Content and Ferulate Cross-Linking than by Lignin Composition. *Journal of the Science of Food and Agriculture*, *89*(1), 122-129.

Hatfield, R., Ralph, J., & Grabber, J. H. (2008). A Potential Role for Sinapyl *p*-Coumarate as a Radical Transfer Mechanism in Grass Lignin Formation. *Planta*, *228*(6), 919-928.

Hatfield, R. D., Grabber, J., Ralph, J., & Brei, K. (1999). Using the acetyl bromide assay to determine lignin concentrations in herbaceous plants: some cautionary notes. *Journal of Agricultural and Food Chemistry*, *47*(2), 628-632.

Hatfield, R. D., Marita, J. M., Frost, K., Grabber, J., Ralph, J., Lu, F., & Kim, H. (2009). Grass Lignin Acylation: *p*-Coumaroyl Transferase Activity and Cell Wall Characteristics of C3 and C4 Grasses. *Planta*, *229*(6), 1253-1267.

Hatfield, R. D., Rancour, D. M., & Marita, J. M. (2017). Grass Cell Walls: A Story of cross-Linking. *Frontiers in plant science*, *7*, 2056.

Hefni, M. E., Amann, L. S., & Witthöft, C. M. (2019). A HPLC-UV Method for the Quantification of Phenolic Acids in Cereals. *Food Analytical Methods*, *12*(12), 2802-2812.

Hemdane, S., Jacobs, P. J., Dornez, E., Verspreet, J., Delcour, J. A., & Courtin, C. M. (2016). Wheat (*Triticum aestivum* L.) Bran in Bread Making: A Critical Review. *Comprehensive Reviews in Food Science and Food Safety*, *15*(1), 28-42.

Hu, Y., Ding, M., Sampson, L., Willett, W. C., Manson, J. E., Wang, M., Rosner, B., Hu, F. B., & Sun, Q. (2020). Intake of Whole Grain Foods and Risk of Type 2 Diabetes: Results from Three Prospective Cohort Studies. *BMJ*, *370*, m2206.

Hullings, A. G., Sinha, R., Liao, L. M., Freedman, N. D., Graubard, B. I., & Loftfield, E. (2020). Whole Grain and Dietary Fiber Intake and Risk of Colorectal Cancer in the NIH-AARP Diet and Health Study cohort. *The American Journal of Clinical Nutrition*, *112*(3), 603-612.

Izydorczyk, M. S., & Biliaderis, C. G. (1995). Cereal Arabinoxylans: Advances in Structure and Physicochemical Properties. *Carbohydrate Polymers*, *28*(1), 33-48.

Jensen, M. K., Koh-Banerjee, P., Hu, F. B., Franz, M., Sampson, L., Gronbaek, M., & Rimm, E. B. (2004). Intakes of Whole Grains, Bran, and Germ and the Risk of Coronary Heart Disease in Men. *The American Journal of Clinical Nutrition*, *80*, 1492-1499.

Jilek, M. L., & Bunzel, M. (2013). Dehydrotriferulic and Dehydrodiferulic Acid Profiles of Cereal and Pseudocereal Flours. *Cereal Chemistry*, *90*(5), 507-514v.

Joyce, G. E., Kagan, I. A., Flythe, M. D., Davis, B. E., & Schendel, R. R. (2023). Profiling of Cool-Season Forage Arabinoxylans via a Validated HPAEC-PAD Method. *Frontiers in plant science*, *14*.

Jung, H. G., & Deetz, D. A. (1993). Cell Wall Lignification and Degradability. In *Forage Cell Wall Structure and Digestibility* (pp. 315-346).

Jung, H. J., Samac, D. A., & Sarath, G. (2012). Modifying Crops to Increase Cell Wall Digestibility. *Plant Science*, *185-186*, 65-77.

Kabel, M. A., Schols, H. A., & Voragen, A. G. J. (2003). Identification of Structural Features of Various (*O*-Acetylated) Xylo-Oligosaccharides from Xylan-Rich

Agricultural By-Products: A Review. In *Hemicelluloses: Science and Technology* (Vol. 864, pp. 107-121). American Chemical Society

Kasuya, N., Xu, Q., Kobayashi, Y., Fukuda, K., Enishi, O., Iiyama, K., & Itabashi, H. (2008). Cell Wall Degradation of Tropical and Temperate Forage Grasses Measured by Nylon Bag and *In Vitro* Digestion Techniques. *Animal Science Journal*, *79*(2), 200-209.

Krause, D. O., Denman, S. E., Mackie, R. I., Morrison, M., Rae, A. L., Attwood, G. T., & McSweeney, C. S. (2003). Opportunities to Improve Fiber Degradation in the Rumen: Microbiology, Ecology, and Genomics. *FEMS Microbiology Reviews*, *27*(5), 663-693.

Lam, T. B., Iiyama, K., & Stone, B. A. (2003). Hot Alkali-Labile Linkages in the Walls of the Forage Grass *Phalaris aquatica* and *Lolium perenne* and their Relation to *In Vitro* Wall Digestibility. *Phytochemistry*, *64*(2), 603-607.

Li, F., Ren, S., Zhang, W., Xu, Z., Xie, G., Chen, Y., Tu, Y., Li, Q., Zhou, S., Li, Y., Tu, F., Liu, L., Wang, Y., Jiang, J., Qin, J., Li, S., Li, Q., Jing, H. C., Zhou, F., Gutterson, N., & Peng, L. (2013). Arabinose Substitution Degree in Xylan Positively affects Lignocellulose Enzymatic Digestibility after Various $NaOH/H_2SO_4$ Pretreatments in *Miscanthus*. *Bioresource Technology*, *130*, 629-637.

Li, S., Morris, C. F., & Bettge, A. D. (2009). Genotype and Environment Variation for Arabinoxylans in Hard Winter and Spring Wheats of the U.S. Pacific Northwest. *Cereal Chemistry*, *86*, 88-95.

Lindgren, E., & Aman, P. (1983). Chemical Composition and *In Vitro* Degradability of Individual Chemical Constituents of Six Swedish Grasses Harvested at Different Stages of Maturity. *Swedish Journal of Agricultural Research*, *13*, 221-227.

Lindgren, E., Theander, O., & Aman, P. (1980). Chemical Compositions of Timothy at Different Stages of Maturity and of Residues from Feeding Value Determinations. *Swedish Journal of Agricultural Research*, *10*, 3-10.

Liu, Q., Luo, L., & Zheng, L. (2018). Lignins: Biosynthesis and Biological Functions in Plants. *International Journal of Molecular Sciences*, *19*(2).

Lombard, V., Golaconda Ramulu, H., Drula, E., Coutinho, P. M., & Henrissat, B. (2014). The Carbohydrate-Active Enzymes
Database (CAZy) in 2013. *Nucleic acids research*, *42*(D1), D490-D495.

Lorenzo, M., Pinedo, M. L., Equiza, M. A., Fernandez, P. V., Ciancia, M., Ganem, D. G., & Tognetti, J. A. (2018). Changes in Apoplastic Peroxidase Activity and Cell Wall Composition are Associated with Cold-Induced Morpho-Anatomical Plasticity of Wheat Leaves. *Plant BIology*, *21 Suppl 1*, 84-94.

Lu, F., & Ralph, J. (1999). Detection and Determination of *p*-Coumaroylated Units in Lignins. *Journal of Agricultural and Food Chemistry*, *47*(5), 1988-1992.

Lynch, K. M., Strain, C. R., Johnson, C., Patangia, D., Stanton, C., Koc, F., Gil-Martinez, J., O'Riordan, P., Sahin, A. W., Ross, R. P., & Arendt, E. K. (2021). Extraction and Characterisation of Arabinoxylan from Brewers Spent Grain and Investigation of Microbiome Modulation Potential. *European Journal of Nutrition*, *60*(8), 4393-4411.

Makaravicius, T., Basinskiene, L., Juodeikiene, G., van Gool, M. P., & Schols, H. A. (2012). Production of Oligosaccharides from Extruded Wheat and Rye Biomass using Enzymatic Treatment. *Catalysis Today*, *196*(1), 16-25.

Marcotuli, I., Hsieh, Y. S., Lahnstein, J., Yap, K., Burton, R. A., Blanco, A., Fincher, G. B., & Gadaleta, A. (2016). Structural Variation and Content of Arabinoxylans in Endosperm and Bran of Durum Wheat (T*riticum turgidum* L.). *Journal of Agricultural and Food Chemistry*, *64*(14), 2883-2892.

Mazumder, K., & York, W. S. (2010). Structural Analysis of Arabinoxylans Isolated from Ball-Milled Switchgrass Biomass. *Carbohydrate Research*, *345*(15), 2183-2193.

McCleary, B. V., McKie, V. A., Draga, A., Rooney, E., Mangan, D., & Larkin, J. (2015). Hydrolysis of Wheat Flour Arabinoxylan, Acid-Debranched Wheat Flour Arabinoxylan and Arabino-Xylo-Oligosaccharides by beta-Xylanase, alpha-L-Arabinofuranosidase and beta-Xylosidase. *Carbohydrate Research*, *407*, 79-96.

McDougall, G. J., Morrison, I. M., Stewart, D., & Hillman, J. R. (1996). Plant Cell Walls as Dietary Fibre: Range, Structure, Processing and Function. *Journal of the Science of Food and Agriculture*, *70*, 133-150.

Morrison, I. M. (1974). Changes in the Hemicellulosic Polysaccharides of Rye-Grass with Increasing Maturity. *Carbohydrate Research*, *36*, 45-51.

Morrison, I. M. (1980). Changes in the Lignin and Hemicellulose Concentrations of Ten Varieties of Temperate Grasses with Increasing Maturity. *Grass and Forage Science*, *35*(4), 287-293.

Murphy, N., Norat, T., Ferrari, P., Jenab, M., Bueno-de-Mesquita, B., Skeie, G., Dahm, C. C., Overvad, K., Olsen, A., Tjonneland, A., Clavel-Chapelon, F., Boutron-Ruault, M. C., Racine, A., Kaaks, R., Teucher, B., Boeing, H., Bergmann, M. M., Trichopoulou, A., Trichopoulos, D., Lagiou, P., Palli, D., Pala, V., Panico, S., Tumino, R., Vineis, P., Siersema, P., van Duijnhoven, F., Peeters, P. H., Hjartaker, A., Engeset, D., Gonzalez, C. A., Sanchez, M. J., Dorronsoro, M., Navarro, C., Ardanaz, E., Quiros, J. R., Sonestedt, E., Ericson, U., Nilsson, L., Palmqvist, R., Khaw, K. T., Wareham, N., Key, T. J., Crowe, F. L., Fedirko, V., Wark, P. A., Chuang, S. C., & Riboli, E. (2012). Dietary Fibre Intake and Risks of

Cancers of the Colon and Rectum in the European Prospective Investigation into Cancer and Nutrition (EPIC). *PLoS One*, *7*(6), e39361.

Neumuller, K. G., Streekstra, H., Gruppen, H., & Schols, H. A. (2014). *Trichoderma longibrachiatum* Acetyl Xylan Esterase 1 Enhances Hemicellulolytic Preparations to Degrade Corn Silage Polysaccharides. *Bioresource Technology*, *163*, 64-73.

Neyrinck, A. M., Possemiers, S., Druart, C., Van de Wiele, T., De Backer, F., Cani, P. D., Larondelle, Y., & Delzenne, N. M. (2011). Prebiotic Effects of Wheat Arabinoxylan Related to the Increase in *Bifidobacteria, Roseburia* and *Bacteroides/Prevotella* in Diet-Induced Obese Mice. *PLoS One*, *6*(6), e20944.

Nyström, L., Lampi, A.-M., Andersson, A. A. M., Kamal-Eldin, A., Gebruers, K., Courtin, C. M., Delcour, J. A., Li, L., Ward, J. L., Fraś, A., Boros, D., Rakszegi, M., Bedő, Z., Shewry, P. R., & Piironen, V. (2008). Phytochemicals and Dietary Fiber Components in Rye Varieties in the HEALTHGRAIN Diversity Screen. *Journal of Agricultural and Food Chemistry*, *56*(21), 9758-9766.

Obel, N., Porchia, A. C., & Scheller, H. V. (2002). Dynamic Changes in Cell Wall Polysaccharides During Wheat Seedling Development. *Phytochemistry*, *60*, 603-610.

Paesani, C., Sciarini, L. S., Moiraghi, M., Salvucci, E., Prado, S. B. R., Pérez, G. T., & Fabi, J. P. (2020). Human Colonic *In Vitro* Fermentation of Water-Soluble Arabinoxylans from Hard and Soft Wheat Alters *Bifidobacterium* Abundance and Short-Chain Fatty Acids Concentration. *LWT - Food Science and Technology*, *134*.

Pareyt, B., & Delcour, J. A. (2008). The Role of Wheat Flour Constituents, Sugar, and Fat in Low Moisture Cereal Based Products: A Review on Sugar-snap Cookies. *Critical Reviews in Food Science and Nutrition*, *48*(9), 824-839.

Pell, G., Szabo, L., Charnock, S. J., Xie, H., Gloster, T. M., Davies, G. J., & Gilbert, H. J. (2004). Structural and Biochemical Analysis of Cellvibrio japonicus Xylanase 10C: How Variation in Substrate-Binding Cleft Influences the Catalytic Profile of Family GH-10 Xylanases. *Journal of Biological Chemistry*, *279*(12), 11777-11788.

Pollet, A., Delcour, J. A., & Courtin, C. M. (2010). Structural Determinants of the Substrate Specificities of Xylanases from dDfferent Glycoside Hydrolase Families. *Critical Reviews in Biotechnology*, *30*(3), 176-191.

Rakszegi, M., Lovegrove, A., Balla, K., Lang, L., Bedo, Z., Veisz, O., & Shewry, P. R. (2014). Effect of Heat and Drought Stress on the Structure and Composition of Arabinoxylan and Beta-Glucan in Wheat Grain. *Carbohydrate Polymers*, *102*, 557-565.

Rancour, D. M., Marita, J. M., & Hatfield, R. D. (2012). Cell Wall Composition throughout Development for the Model Grass *Brachypodium distachyon*. *Frontiers in plant science*, *3*, 266.

Rogowski, A., Briggs, J. A., Mortimer, J. C., Tryfona, T., Terrapon, N., Lowe, E. C., Basle, A., Morland, C., Day, A. M., Zheng, H., Rogers, T. E., Thompson, P., Hawkins, A. R., Yadav, M. P., Henrissat, B., Martens, E. C., Dupree, P., Gilbert, H. J., & Bolam, D. N. (2015). Glycan Complexity Dictates Microbial Resource Allocation in the Large Intestine. *Nature communications*, *6*, 7481.

Saeman, J. F., Bubl, J. L., & Harris, E. E. (1945). Quantitative Saccharification of Wood and Cellulose. *Industrial & Engineering Chemistry Analytical Edition*, *17*(1), 35-37.

Saulnier, L., Guillon, F., & Chateigner-Boutin, A.-L. (2012). Cell Wall Deposition and Metabolism in Wheat Grain. *Journal of Cereal Science*, *56*(1), 91-108.

Schadel, C., Blochl, A., Richter, A., & Hoch, G. (2010). Quantification and Monosaccharide Composition of Hemicelluloses from Different Plant Functional Types. *Plant Physiology and Biochemistry*, *48*(1), 1-8.

Scheller, H. V., & Ulvskov, P. (2010). Hemicelluloses. *Annual Review of Plant Biology*, *61*, 263-289.

Schendel, R. R., Meyer, M. R., & Bunzel, M. (2016). Quantitative Profiling of Feruloylated Arabinoxylan Side-Chains from Graminaceous Cell Walls. *Frontiers in plant science*, *6*, 1249.

Schmitz, E., Nordberg Karlsson, E., & Adlercreutz, P. (2020). Warming Weather Changes the Chemical Composition of Oat Hulls. *Plant BIology*, *22*(6), 1086-1091.

Selig, M. J., Thygesen, L. G., Felby, C., & Master, E. R. (2015). Debranching of Soluble Wheat Arabinoxylan Dramatically Enhances Recalcitrant Binding to Cellulose. *Biotechnology Letters*, *37*(3), 633-641.

Selvendran, R. R., March, J. F., & Ring, S. G. (1979). Determination of Aldoses and Uranic Acid Content of Vegetable Fiber. *Analytical Biochemistry*, *96*, 282-292.

Shewry, P. R., Piironen, V., Lampi, A. M., Edelmann, M., Kariluoto, S., Nurmi, T., Fernandez-Orozco, R., Andersson, A. A., Aman, P., Fras, A., Boros, D., Gebruers, K., Dornez, E., Courtin, C. M., Delcour, J. A., Ravel, C., Charmet, G., Rakszegi, M., Bedo, Z., & Ward, J. L. (2010). Effects of Genotype and Environment on the Content and Composition of Phytochemicals and Dietary Fiber Components in Rye in the HEALTHGRAIN Diversity Screen. *Journal of Agricultural and Food Chemistry*, *58*(17), 9372-9383.

Sousa, D. O., Murphy, M., Hatfield, R., & Nadeau, E. (2021). Effects of Harvest Date and Grass Species on Silage Cell Wall Components and Lactation pPerformance of Dairy Cows. *Journal of dairy science*, *104*(5), 5391-5404.

Suen, G., Weimer, P. J., Stevenson, D. M., Aylward, F. O., Boyum, J., Deneke, J., Drinkwater, C., Ivanova, N. N., Mikhailova, N., Chertkov, O., Goodwin, L. A., Currie, C. R., Mead, D., & Brumm, P. J. (2011). The Complete Genome Sequence of *Fibrobacter succinogenes* S85 Reveals a Cellulolytic and Metabolic Specialist. *PLoS One*, *6*(4), e18814.

Toole, G. A., Le Gall, G., Colquhoun, I. J., Johnson, P., Bedo, Z., Saulnier, L., Shewry, P. R., & Mills, E. N. (2011). Spectroscopic Analysis of Diversity of Arabinoxylan Structures in Endosperm Cell Walls of Wheat Cultivars (*Triticum aestivum*) in the HEALTHGRAIN Diversity Collection. *Journal of Agricultural and Food Chemistry*, *59*(13), 7075-7082.

Turner, L. B., Mueller-Harvey, I., & McAllan, A. B. (1991). Light-Induced Isomerization and Dimerization of Cinnamic Acid Dervitatives in Cell Walls. *Phytochemistry.*, *33*(4), 791-796.

Vaidyanathan, S., & Bunzel, M. (2012). Development and Application of a Methodology to Determine Free Ferulic Acid and Ferulic Acid Ester-Linked to Different Types of Carbohydrates
in Cereal Products. *Cereal Chemistry*, *89*(5), 247-254.

Van Soest, P. J., & Wine, R. H. (1967). Use of Detergents in the Analysis of Fibrous Feeds. IV. Determination of Plant Cell-Wall Constituents. *Journal of Association of Official Analytical Chemists*, *50*(1), 50-55.

Veličković, D., Ropartz, D., Guillon, F., Saulnier, L., & Rogniaux, H. (2014). New Insights into the Structural and Spatial Variability of Cell-Wall Polysaccharides During Wheat Grain Development, as Revealed Through MALDI Mass Spectrometry Imaging. *Journal of Experimental Botany*, *65*(8), 2079-2091.

Verbruggen, M. A., Spronk, B. A., Schols, H. A., Beldman, G., Voragen, A. G. J., Thomas, J. R., Kamerling, J. P., & Vliegenthart, J. F. G. (1998). Structures of Enzymically Derived Oligosaccharides from Sorghum Glucuronoarabinoxylan. *Carbohydrate Research*, *306*(1), 265-274.

Viëtor, R. J., Hoffmann, R. A., Angelino, S. A. G. F., Voragen, A. G. J., Kamerling, J. P., & Vliegenthart, J. F. G. (1994). Structures of Small Oligomers Liberated from Barley Arabinocylans by Endoxylanase from *Aspergillus awamori*. *Carbohydrate Research*, *254*, 245-255.

Wallsten, J., & Hatfield, R. (2016). Cell Wall Chemical Characteristics of Whole-Crop Cereal Silages Harvested at Three Maturity Stages. *Journal of the Science of Food and Agriculture*, *96*(10), 3604-3612.

Weickert, M. O., & Pfeiffer, A. F. H. (2018). Impact of Dietary Fiber Consumption on Insulin Resistance and the Prevention of Type 2 Diabetes. *The Journal of Nutrition*, *148*(1), 7-12.

Withers, S., Lu, F., Kim, H., Zhu, Y., Ralph, J., & Wilkerson, C. G. (2012). Identification of Grass-Specific Enzyme that Acylates Monolignols with *p*-Coumarate. *The Journal of Biological Chemistry*, *287*(11), 8347-8355.

Xu, F., Sun, J. X., Geng, Z. C., Liu, C. F., Ren, J. L., Sun, R. C., Fowler, P., & Baird, M. S. (2007). Comparative Study of Water-Soluble and Alkali-Soluble Hemicelluloses from Perennial Ryegrass leaves (*Lolium perenne*). *Carbohydrate Polymers*, *67*(1), 56-65.

Zannini, E., Bravo Nunez, A., Sahin, A. W., & Arendt, E. K. (2022). Arabinoxylans as Functional Food Ingredients: A Review. *Foods*, *11*(7).

Vita
Sophia Danielle Newhuis

Education

Bachelor of Science Degree in Food Science 08/2016-05/2020
University of Kentucky, Lexington, KY

Professional Experience

Graduate Research Assistant 2021-present
Department of Animal & Food Sciences, University of Kentucky
Undergraduate Research Assistant Summer 2019
Department of Animal & Food Sciences, University of Kentucky

Scholarships and Awards

- Animal & Food Sciences Departmental Outstanding M.S Student Award 2022
- Clair L. Hicks Food Science Scholarship 2021-2022
- 3rd place M.S division at AFSGA 10th Annual Poster Symposium 2022

Publications

Master's Thesis – *"Plant cell wall composition and in vitro fermentation characteristics of cool-season forage grasses from two growing seasons in central Kentucky"* (Spring 2023)
Oral presentation -- "*Structural and compositional changes in the cell walls of cool-season pasture grasses for two growing seasons*" - American Chemical Society National Conference Spring 2023, Indianapolis, IN.
Oral presentation-- "*Changes in cell-wall composition of cool-season pasture grasses over the growing season"* - American Chemical Society National Conference Spring 2022, San Diego, CA.
Poster presentation – "*Compositional and structural changes in the cell walls of cool-season pasture forages over the growing season"*- Cereals and Grains Conference Fall 2022, Bloomington, MN.
Poster presentation – *"The release of feruloylated oligosaccharides from distiller's spent grain"* – James B. Beam Institute Conference Spring 2020, Lexington, KY.